

# PLC-mediated PI(4,5)P<sub>2</sub> hydrolysis regulates activation and inactivation of TRPC6/7 channels

Kyohei Itsuki,<sup>1,2</sup> Yuko Imai,<sup>1,2</sup> Hideharu Hase,<sup>3</sup> Yasushi Okamura,<sup>4</sup> Ryuji Inoue,<sup>1</sup> and Masayuki X. Mori<sup>1,3</sup>

<sup>1</sup>Department of Physiology, School of Medicine, Fukuoka University, Fukuoka 814-0180, Japan

<sup>2</sup>Faculty of Dental Science, Kyushu University, Fukuoka 812-8581, Japan

<sup>3</sup>Department of Synthetic Chemistry and Biological Chemistry, Graduate School of Engineering, Kyoto University, Kyoto 615-8501, Japan

<sup>4</sup>Laboratory of Integrative Physiology, Department of Physiology, Graduate School of Medicine, Osaka University, Osaka 565-0871, Japan

Transient receptor potential classical (or canonical) (TRPC)3, TRPC6, and TRPC7 are a subfamily of TRPC channels activated by diacylglycerol (DAG) produced through the hydrolysis of phosphatidylinositol 4,5-bisphosphate (PI(4,5)P<sub>2</sub>) by phospholipase C (PLC). PI(4,5)P<sub>2</sub> depletion by a heterologously expressed phosphatase inhibits TRPC3, TRPC6, and TRPC7 activity independently of DAG; however, the physiological role of PI(4,5)P<sub>2</sub> reduction on channel activity remains unclear. We used Förster resonance energy transfer (FRET) to measure PI(4,5)P<sub>2</sub> or DAG dynamics concurrently with TRPC6 or TRPC7 currents after agonist stimulation of receptors that couple to G<sub>q</sub> and thereby activate PLC. Measurements made at different levels of receptor activation revealed a correlation between the kinetics of PI(4,5)P<sub>2</sub> reduction and those of receptor-operated TRPC6 and TRPC7 current activation and inactivation. In contrast, DAG production correlated with channel activation but not inactivation; moreover, the time course of channel inactivation was unchanged in protein kinase C-insensitive mutants. These results suggest that inactivation of receptor-operated TRPC currents is primarily mediated by the dissociation of PI(4,5)P<sub>2</sub>. We determined the functional dissociation constant of PI(4,5)P<sub>2</sub> to TRPC channels using FRET of the PLC $\delta$  Pleckstrin homology domain (PHd), which binds PI(4,5)P<sub>2</sub>, and used this constant to fit our experimental data to a model in which channel gating is controlled by PI(4,5)P<sub>2</sub> and DAG. This model predicted similar FRET dynamics of the PHd to measured FRET in either human embryonic kidney cells or smooth muscle cells, whereas a model lacking PI(4,5)P<sub>2</sub> regulation failed to reproduce the experimental data, confirming the inhibitory role of PI(4,5)P<sub>2</sub> depletion on TRPC currents. Our model also explains various PLC-dependent characteristics of channel activity, including limitation of maximum open probability, shortening of the peak time, and the bell-shaped response of total current. In conclusion, our studies demonstrate a fundamental role for PI(4,5)P<sub>2</sub> in regulating TRPC6 and TRPC7 activity triggered by PLC-coupled receptor stimulation.

## INTRODUCTION

Transient receptor potential classical/canonical (TRPC) 3, C6, and C7 channels are the closest mammalian homologues of the *Drosophila melanogaster* TRP channel and are expressed in various cell types, including smooth muscle and neurons (Hardie, 2003; Inoue et al., 2006; Venkatachalam and Montell, 2007). These channels conduct cations (Na<sup>+</sup>, Ca<sup>2+</sup>) in response to stimulation of receptors coupled to phospholipase C (PLC), namely G<sub>q</sub> protein-coupled receptors and certain tyrosine kinase receptors (Ramsey et al., 2006). For that reason,

the currents mediated by these channels are often called receptor-operated cation currents (Inoue and Kuriyama, 1993; Firth et al., 2007). TRPC3/6/7 channels are also activated by synthetic membrane-permeable diacylglycerol (DAG) analogues and are thus considered to be DAG-sensitive or activated channels (Hofmann et al., 1999; Okada et al., 1999). In a physiological context, DAG is produced by the hydrolytic activity of PLC, which is located downstream of the receptors for neurotransmitters and hormones. Therefore, the receptor stimulation activates TRPC3/6/7 channels through the production of DAG to generate the receptor-operated TRPC currents (Beech et al., 2004; Panda et al., 2005; Hartmann et al., 2008).

Correspondence to Masayuki X. Mori: mxmori@sbchem.kyoto-u.ac.jp

Abbreviations used in this paper: AVP, arginine<sup>8</sup> vasopressin; CCh, carbachol; DAG, diacylglycerol; DrVSP, *Danio rerio* voltage-sensing phosphatase; FR, Förster resonance energy transfer ratio; FRET, Förster resonance energy transfer; HEK, human embryonic kidney; IP<sub>3</sub>, inositol 1,4,5-trisphosphate; M<sub>1</sub>R, muscarinic type 1 receptor; PA, phosphatidic acid; PHd, Pleckstrin homology domain; PI(4,5)P<sub>2</sub>, phosphatidylinositol 4,5-bisphosphate; PIP5K, phosphatidylinositol-4-phosphate-5-kinase; PLC, phospholipase C; SPD, self-limiting regulation by PI(4,5)P<sub>2</sub>-DAG signaling; TRPC, transient receptor potential classical/canonical.

© 2014 Itsuki et al. This article is distributed under the terms of an Attribution-Noncommercial-Share Alike-No Mirror Sites license for the first six months after the publication date (see <http://www.rupress.org/terms>). After six months it is available under a Creative Commons License (Attribution-Noncommercial-Share Alike 3.0 Unported license, as described at <http://creativecommons.org/licenses/by-nc-sa/3.0/>).

Phosphatidylinositol 4,5-bisphosphate (PI(4,5)P<sub>2</sub>, or PIP<sub>2</sub>) is the major substrate of PLC, and its hydrolysis produces DAG. PI(4,5)P<sub>2</sub> is known to regulate numerous ion channels, modulating electrical signal outputs from metabotropic receptors in diverse physiological contexts (Gamper and Shapiro, 2007; Hilgemann, 2007; Logothetis et al., 2007). However, knowledge concerning the effect of PI(4,5)P<sub>2</sub> on TRPC channels is still accumulating (Jardín et al., 2008; Lemonnier et al., 2008; Monet et al., 2012). We have recently demonstrated using *Danio rerio* voltage-sensing phosphatase (DrVSP) that reduction or depletion of PI(4,5)P<sub>2</sub> inhibits the activity of DAG-sensitive TRPC3/6/7 channels, both in an exogenous expression system and in smooth muscle-derived cells (A7r5) (Imai et al., 2012; Itsuki et al., 2012a). The DrVSP-mediated inhibition of TRPC3/6/7 currents was detected even in currents evoked by a membrane-permeable DAG analogue (OAG), which suggests that reduction in PI(4,5)P<sub>2</sub> can inhibit TRPC3/6/7 channel opening regardless of the presence of DAG. Under G<sub>q</sub> protein-coupled receptor stimulation, PI(4,5)P<sub>2</sub> hydrolysis (breakdown) by the receptor-activated PLC largely contributes to the production of DAG. Therefore, such a complex relationship of PI(4,5)P<sub>2</sub> and DAG suggests that TRPC3/6/7 channel activity may be regulated in a self-limiting manner.

The effects of PLC-coupled receptor-driven channel regulation via enzymatic hydrolysis of PI(4,5)P<sub>2</sub> are not known. To improve our understanding, we simultaneously measured PI(4,5)P<sub>2</sub> or DAG dynamics and receptor-operated TRPC currents evoked by carbachol (CCh; a muscarinic receptor agonist) or vasopressin (a vasoconstrictor). To this end, we measured the levels of PI(4,5)P<sub>2</sub> and DAG using a quantitative Förster resonance energy transfer (FRET)-based sensor alongside detection of TRPC6 and TRPC7 currents, which are more sensitive than TRPC3 currents to reduction in PI(4,5)P<sub>2</sub> in human embryonic kidney (HEK)293 cells and smooth muscle-derived cells. We found that the temporal FRET dynamics of PI(4,5)P<sub>2</sub> reduction closely correlate with the time course of activation and inactivation of receptor-operated TRPC6/7 channel currents. We also constructed a kinetic model of receptor-driven PI(4,5)P<sub>2</sub>-DAG signaling. This model, calibrated with DrVSP-derived functional dissociation constants for PI(4,5)P<sub>2</sub> binding to TRPC3/6/7 channels, closely resembled our experimental results. Our study, combining experimental and computer simulation data, revealed the crucial role of receptor-stimulated PI(4,5)P<sub>2</sub> hydrolysis in TRPC6/7 currents. Part of the work presented here has appeared in abstract form (Itsuki et al., 2012b).

## MATERIALS AND METHODS

### Plasmids and cells

The pcDNA3 expression vector encoding human TRPC6 (GenBank accession no. NM\_004621) was provided by T. Hofmann

(Institut für Pharmakologie und Toxikologie, Zürich, Switzerland); pCI-neo expression vectors encoding mouse TRPC3 (GenBank accession no. NM\_019510) and TRPC7 (GenBank accession no. NM\_012035) were provided by Y. Mori (Kyoto University, Kyoto, Japan). Single amino acid mutation in TRPC6 and TRPC7 was generated using the QuikChange Site-Directed Mutagenesis kit (Agilent Technologies) according to the manufacturer's instructions. To generate bright FRET pairs, super-enhanced YFP or CFP isolated from a RhoA FRET sensor (provided by M. Matsuda, Kyoto University, Kyoto, Japan) were modified to give A207K mutants as a monomeric form (CFP<sub>msc</sub> or YFP<sub>msc</sub>) (Zacharias et al., 2002). These modified fluorophores were fused to the N-terminal side of the PLC $\delta$  Pleckstrin homology domain (PHd; provided by K. Jalink, The Netherlands Cancer Institute, Amsterdam, Netherlands) to construct PI(4,5)P<sub>2</sub> sensor molecules consisting of CFP<sub>msc</sub>-PHd or YFP<sub>msc</sub>-PHd. For DAG detection, CFP<sub>msc</sub> was fused to the C-terminal side of PKC $\epsilon$  (provided by M. Schaefer, Leipzig University, Leipzig, Germany), yielding PKC $\epsilon$ -CFP<sub>msc</sub>. To be an energy acceptor of membrane-bound PKC $\epsilon$ -CFP<sub>msc</sub>, YFP<sub>msc</sub> was attached to the C-terminal side of the GAP-43 myristoyl domain (Invitrogen) through an octaglycine (G8) linker (Myr-YFP<sub>msc</sub>). PI(4,5)P<sub>2</sub> and DAG sensor cDNA were each incorporated into an IRES-reporter region-excluded pIRES2 expression vector (Invitrogen). A pEF-BOS expression vector encoding human muscarinic type 1 receptor (M<sub>1</sub>R) was provided by T. Haga (Gakushuin University, Tokyo, Japan). Human phosphatidylinositol-4-phosphate-5-kinase (PIP5K;  $\beta$  isoform) in pcDNA3.1 vector (Invitrogen) was provided by S. Kita and T. Iwamoto (Fukuoka University, Fukuoka, Japan). All PCR products were sequenced entirely.

HEK293 cells (obtained from the ATCC) were maintained in Dulbecco's modified Eagle's medium (Invitrogen) supplemented with 10% FBS (Gibco) and antibiotics (penicillin and streptomycin; Gibco) at 37°C (5% CO<sub>2</sub>). For transfection, cells were seeded on poly-L-lysine-coated glass coverslips (Matsunami) in 35-mm culture dishes and transfected with a mixture of plasmid vector-incorporated DNAs using the SuperFect transfection reagent (QIAGEN). For FRET-based PI(4,5)P<sub>2</sub> detection, HEK293 cells were cotransfected with 1  $\mu$ g each of plasmids encoding TRPC3, 6, or 7 together with M<sub>1</sub>R (or without it, in endogenous muscarinic receptor stimulation) and 0.3  $\mu$ g each of plasmids encoding CFP<sub>msc</sub>-PHd and YFP<sub>msc</sub>-PHd. For DAG detection, 0.3  $\mu$ g each of plasmids encoding Myr-YFP<sub>msc</sub> and PKC $\epsilon$ -CFP<sub>msc</sub> were cotransfected instead of the PI(4,5)P<sub>2</sub> sensor plasmids. For detection of local PI(4,5)P<sub>2</sub> around the TRPC7 channel, the sequence encoding the donor protein (CFP<sub>msc</sub>) was inserted before the stop codon of TRPC7. In this case, equal amounts (1  $\mu$ g) of donor, acceptor (YFP<sub>msc</sub>-PHd), and M<sub>1</sub>R plasmids were used for transfection. Measurements on transfected cells were made within 24–72 h after transfection.

A7r5 cells, the cell line derived from rat thoracic aortic smooth muscle (Brandt et al., 1976), were obtained from the ATCC, maintained in medium identical to that used for HEK293 cells, and passaged every 5–7 d. The transfection protocol was essentially the same as the one used with HEK293 cells. A7r5 cells transfected with CFP<sub>msc</sub>-PHd and YFP<sub>msc</sub>-PHd were reseeded on poly-L-lysine-coated glass coverslips and incubated at 37°C (5% CO<sub>2</sub>) for at least 15 min before use. Cells were always used within 2 h of reseeded.

### Solutions and drugs

The standard external solution contained (mM): 140 NaCl, 5 KCl, 1 CaCl<sub>2</sub>, 1.2 MgCl<sub>2</sub>, 10 HEPES, and 10 glucose (pH 7.4, adjusted with Tris base; 300 mOsm, adjusted with glucose). The pipette solution contained (mM): 120 CsOH, 120 aspartate, 20 CsCl, 2 MgCl<sub>2</sub>, 5 EGTA, 1.5 CaCl<sub>2</sub>, 10 HEPES, 2 ATP-Na<sub>2</sub>, 0.1 GTP, and 10 glucose (pH 7.2, adjusted with Tris base; 290–295 mOsm, adjusted with glucose). CCh (Sigma-Aldrich) was diluted in the standard

external solution from its stock concentration (100 mM in H<sub>2</sub>O). To confirm monovalent cationic currents, NMDG solution (150 mM *N*-methyl-D-glucamine chloride, 10 mM HEPES, and 1 mM CaCl<sub>2</sub>, with pH 7.4 adjusted with HCl) was applied at the end of each stimulus. RHC80267 (EMD Millipore) was dissolved in DMSO (Wako Chemicals USA). Stock solutions of Arginine<sup>8</sup> vasopressin (AVP; 100 μM; MP Biomedicals) and nifedipine (10 mM; EMD Millipore) were dissolved in H<sub>2</sub>O and DMSO, respectively. AVP and nifedipine were freshly prepared in the standard external solution to final concentrations of 1 and 5 μM, respectively, before applying to A7r5 cells. During experiments, HEK293 and A7r5 cells were continuously perfused with external solution and gravity-fed at a flow rate of 0.25 ml/min. The perfusion was turned on and off using electromagnetic solenoid microvalves (The Lee Co.).

### Simultaneous measurements of TRPC currents and FRET

**Electrophysiology.** The whole-cell patch-clamp technique was used for current detection. Patch electrodes with a resistance of 4–6 MΩ (when filled with internal solution) were made from 1.5-mm borosilicate glass capillaries (Sutter Instrument). Series resistance errors were compensated >60%. Voltage generation and current signal acquisition were accomplished using a patch-clamp amplifier (AxpPatch 200B; Axon Instruments) with an A/D D/A converter (Digidata 1200; Axon Instruments). Sampled data were low-pass filtered and digitized at 1 kHz using pClamp 9.0 (Axon Instruments) and analyzed using custom-written software (MATLAB; MathWorks). The currents were recorded at a holding potential of −50 mV. For activation of DrVSP, depolarizing step pulses (from 20 to 180 mV, 500-ms duration) were delivered every 20 s. The ratio of the currents before and after DrVSP activation was used to quantitate DrVSP-mediated inhibition, “*r* (*I*).” Before its calculation, the leak that was defined by the current in NMDG-containing solution was subtracted. All experiments were performed at room temperature (22–25°C).

**FRET detection.** Fluorescence from voltage-clamped cells was detected using a microscope (60 × 0.9 N.A. objective; TE300 Eclipse; Nikon) equipped with a two-channel simultaneous beam-splitter (Dual-View2; Photometrics) and a high sensitivity EMCCD camera (Evolve512; Photometrics). Excitation light filtered at 427/10 and 504/12 nm was alternately introduced via an optical fiber from a lamp house equipped with a high speed excitation wavelength selector (75 W xenon lamp; OSP-EXA; Olympus). Epifluorescence from the cells was prefiltered using a multiband dichroic mirror (449–483 and 530–569 nm) contained in the microscope, and then further separated in the beam-splitter (at 505 nm) and filtered at 464/23 nm (detection of the donor fluorescence) or 542/27 nm (detection of the acceptor fluorescence). Optical filters were obtained from Semrock, except the splitter (Chroma Technology Corp.). The duration of camera exposure was 100 ms and occurred within 150-ms periods of illumination at each excitation wavelength. Images were captured with an EM gain of 300 and then digitized as 512 × 512 pixels by 16-bit arrays in the microscope software (Micro-manager v.1.4). The image pixel resolution was ~0.26 μm. Averaged intensities from the whole-cell region (typically 20 × 20 to 40 × 40 square pixels) were analyzed to calculate FRET using a custom-written MATLAB program. The electrophysiology and FRET measurements were synchronized using brief triggers from the A/D D/A converter linked to the excitation light shutter. All of the data in this paper were recorded from the first application of any of the agonists.

**Calculation of FRET.** Fluorescence signal output obtained from a given sample is denoted by the descriptor  $F_{X(Y)}$ , where X and Y are the fluorescence filter settings for the emission and excitation light, respectively. The emission filter for donor fluorescence (464 nm)

is denoted as “464,” and that for acceptor fluorescence (542 nm) as “542.” The excitation filter for donor excitation (427 nm) is denoted as “D,” and that for acceptor excitation (504 nm) as “A.” Background intensity, captured using the corresponding filter setting with nontransfected cells, was subtracted from specimen fluorescence signals. Finally, the FRET ratio (*FR*) was calculated according to the “3-cube” method (Erickson et al., 2001):

$$FR = (F_{542(D)} - RD1 \cdot F_{464(D)}) / RA \cdot (F_{542(A)} - RD2 \cdot F_{542(D)}), \quad (1)$$

where  $RD1 = F_{542(D)}/F_{464(D)}$ ,  $RD2 = F_{542(A)}/F_{464(D)}$ , and  $RA = F_{542(D)}/F_{542(A)}$ . Constants of *RD1*, *RD2*, and *RA* were predetermined using measurements from single cells expressing only donor- (CFP<sub>msc</sub>) and acceptor- (YFP<sub>msc</sub>) tagged molecules, respectively. From the *FR* values, we can compute the effective FRET efficiency ( $E_{EFF}$ ):

$$E_{EFF} = (FR - 1) \cdot [\epsilon YFP_{msc}(427) / \epsilon CFP_{msc}(427)], \quad (2)$$

where  $\epsilon YFP_{msc}$  and  $\epsilon CFP_{msc}$  are the molar extinction coefficients for the FRET cube excitation filters obtained using the 427-nm excitation band-pass filter. We determined the ratio in brackets to be 0.11, based on maximal extinction coefficients for YFP<sub>msc</sub> and CFP<sub>msc</sub> (Mori et al., 2011).

### Establishment of a relationship between PI(4,5)P<sub>2</sub> concentration and FRET

Here, we calculated the relationship between FRET and PI(4,5)P<sub>2</sub>. To this end, we considered two different cases: (1) FRET between TRPC7 channel-anchored CFP<sub>msc</sub> and YFP<sub>msc</sub>-PHd, where YFP<sub>msc</sub>-PHd can transit between a soluble cytoplasmic state and a PI(4,5)P<sub>2</sub>-bound membrane state; and (2) FRET between CFP<sub>msc</sub>-PHd and YFP<sub>msc</sub>-PHd, where both probes transition between a soluble and membrane-bound state.

Case 1 is described by:

$$\frac{FR}{FR_{max}} \approx F = \frac{1}{1 + \frac{K_d(PHD)}{[PI(4,5)P_2]}}, \quad (3)$$

where *F* is the fraction of PHd bound to PI(4,5)P<sub>2</sub>,  $K_d(PHD)$  is the dissociation constant of PHd bound to PI(4,5)P<sub>2</sub> (reported as 2.0 μM; Lemmon et al., 1996; Hirose et al., 1999), and  $FR_{max}$  is the maximum *FR* at an infinitely high concentration of PI(4,5)P<sub>2</sub> that induces all the fluorophore-fused PHd probes to bind to the plasma membrane.  $FR_{max}$  is a purely theoretical value, because physiological PI(4,5)P<sub>2</sub> levels (5–40 μM) are insufficient to localize all PHd proteins to the plasma membrane (Bunce et al., 1993; McLaughlin and Murray, 2005). Nevertheless, although  $FR_{max}$  is impossible to demonstrate, overexpression of PIP5K can greatly increase the cellular levels of PI(4,5)P<sub>2</sub> by approximately two- to threefold (Winks et al., 2005). We observed that cells overexpressing PIP5K demonstrated ~1.2 times higher *FR* than control cells with resting PI(4,5)P<sub>2</sub> levels (Fig. 5 A). We thus calculated the  $FR_{max}$  value by multiplying the resting *FR* by this correction factor of 1.2. Eq. 3 was used to simulate *FR* dynamics in cells expressing TRPC7-CFP<sub>msc</sub> and YFP<sub>msc</sub>-PHd, as shown in Eq. 25 (Table 3) and Fig. 7 D. Conversion of the FRET between CFP<sub>msc</sub>-PHd and YFP<sub>msc</sub>-PHd to PI(4,5)P<sub>2</sub> concentration (i.e., case 2) is described in the Results.

### Estimation of expressed fluorophore-tagged PHd proteins

We determined that the average concentration of fluorophore-tagged PHd in single cells was 1.6 μM. This value was calculated based on the intensity from fluorescein (Sigma-Aldrich) as follows.

Fluorescein was dissolved in 50 mM borate buffer (pH 9.1). The fluorescence intensities in small droplets of this fluorescein solution were measured, under the same conditions as the cells overexpressing YFP<sub>msec</sub>-PHd. The respective intensities were standardized by the quantum yields for fluorescein (0.92) and YFP<sub>msec</sub> (0.57), and then the average [YFP<sub>msec</sub>-PHd] in living cell was determined to be 0.8 μM. Equal amounts of CFP<sub>msec</sub>-PHd and YFP<sub>msec</sub>-PHd plasmids were transfected, so total amounts of CFP<sub>msec</sub>-PHd and YFP<sub>msec</sub>-PHd proteins could be extrapolated from this value.

### Modeling and fitting statistics

Kinetic models of PI(4,5)P<sub>2</sub> hydrolysis pathway by PLC were formulated as ordinary differential equations, and the concentrations of PI(4,5)P<sub>2</sub> and DAG derived from these were incorporated into the channel-operation models. Simulations were performed in Excel (Microsoft) using the forward Euler method with a time step of 0.05 s. Individual steps were translated into differential equations based on the proposed kinetic scheme. Fitting the models to the experimental data of TRPC6/7 currents was performed by a Generalized Reduced Gradient algorithm of the Solver function in Excel. Details of model formulations and model fitting to the experimental data are described in the Results.

The errors between the experimental and the back-calculated *FR* by model fitting to the currents (Figs. 6 and 7) were evaluated by the standard deviations of residual as follows:

$$SD(\sigma) = \sqrt{\sum_{i=0}^n (\text{Norm.}FR - \text{Norm.}FR_{bk})_i^2 / (n-1)},$$

where Norm.*FR* and Norm.*FR*<sub>bk</sub> denote the normalized experimental and back-calculated *FR* at the *i* points. *n* indicates the total number of time points (20/s).

### Online supplemental material

Plotting the currents versus *FR*<sub>min</sub>/*FR*<sub>resting</sub> relationship (Fig. S1). DrVSP-mediated inhibition at the single-channel level (Fig. S2). Diffused PI(4,5)P<sub>2</sub> was incorporated in the self-limiting regulation by PI(4,5)P<sub>2</sub>-DAG signaling (SPD) model-based simulation

(Fig. S3). Incomplete matching of the DG model to the experimental *FR* (Fig. S4). The quick recovery of *FR* under the AVP stimulation (Fig. S5). Fitting the SPD model to TRPC7 current demonstrated less matching to *FR* dynamics and vice versa (Fig. S6). Effect of an inactive ATP analogue in the patch pipette on the receptor-operated TRPC7 currents (Fig. S7). The online supplemental material is available at <http://www.jgp.org/cgi/content/full/jgp.201311033/DC1>.

## RESULTS

### Simultaneous measurement of PI(4,5)P<sub>2</sub> and TRPC currents

The PHd of PLCδ binds both PI(4,5)P<sub>2</sub> and inositol 1,4,5-trisphosphate (IP<sub>3</sub>) (Hirose et al., 1999). In the resting state, however, most of the fluorophore-tagged PHds are located at the plasma membrane, making it possible to measure PI(4,5)P<sub>2</sub> at the plasma membrane (van der Wal et al., 2001; Jensen et al., 2009; Yudin et al., 2011) (Fig. 1 A). Using this approach, we first demonstrated the simultaneous measurements of PI(4,5)P<sub>2</sub> and receptor-operated TRPC6 current. The FRET pairs, which consisted of donor (CFP<sub>msec</sub>) or acceptor (YFP<sub>msec</sub>) fused to the PHd, were coexpressed with TRPC6 channel and M<sub>1</sub>R in mammalian HEK293 cells (Fig. 1 B). Fig. 1 C shows a typical example of the simultaneous measurement of a TRPC6 current and PI(4,5)P<sub>2</sub> levels in a HEK293 cell after stimulation with 10 μM CCh. Soon after CCh application, an inward TRPC6 current (Fig. 1 C, top) and FRET reduction (middle) were observed concurrently.

To evaluate the kinetics of the current activation and inactivation, we measured the time required for receptor-operated TRPC6 current to increase from 10 to 90% of its peak amplitude and then to decay from 90 to 50% (Fig. 1 C, top). We quantitatively examined the real-time

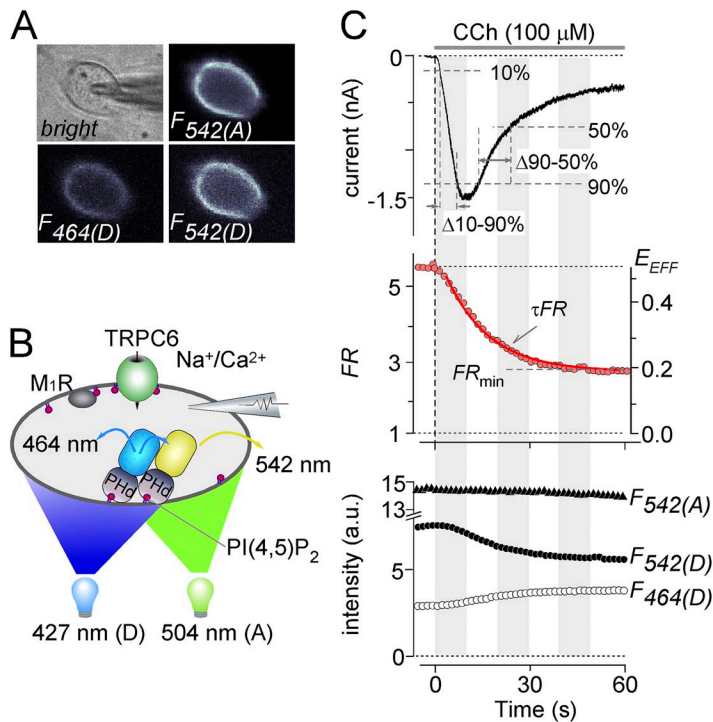


**Figure 1.** Simultaneous measurement of receptor-operated TRPC6 currents and PI(4,5)P<sub>2</sub> detected by 3-cube FRET. (A) Images of PI(4,5)P<sub>2</sub> sensor expressed in HEK293 cells using a 3-cube filter. Phase-contrast image (top left), YFP channel (*F*<sub>542(A)</sub>; top right), CFP channel (*F*<sub>464(D)</sub>; bottom left), and FRET channel (*F*<sub>542(D)</sub>; bottom right) are shown. (B) Diagram of molecules transfected into HEK293 cells. TRPC6, PI(4,5)P<sub>2</sub> sensor (CFP<sub>msec</sub>-PHd [blue box] and YFP<sub>msec</sub>-PHd [yellow box]), and M<sub>1</sub>R were expressed. The excitation wavelengths, 427 and 504 nm, were alternately illuminated. (C) Typical example of CCh-induced TRPC6 currents (top) and the corresponding FRET changes (middle). The *FR* (middle; circles) calculated by 3-cube methods can yield near absolute FRET efficiency (*E*<sub>EFF</sub>; right axis). Measured parameters were the duration of Δ10–90% and Δ90–50% of the peak current, the kinetics of FRET decay (*τFR*), and minimum *FR* (*FR*<sub>min</sub>). The decline of FRET (*FR*) was fitted with a single-exponential decay (red solid curve): *FR* = *FR*<sub>min</sub> + *FR*<sub>Δ</sub> × exp(−*t* / *τFR*). The bottom panel shows the changes in the fluorescence intensities (a.u.) that passed through the respective filter setting.

alteration in PI(4,5)P<sub>2</sub> level using the 3-cube FRET measurement (described in Materials and methods). FRET changes over time between CFP<sub>msec</sub>-PHd and YFP<sub>msec</sub>-PHd (Fig. 1 C, middle) were calculated from the respective fluorescence intensities (Fig. 1 C, bottom). The donor fluorescence (Fig. 1 C, open circles;  $F_{464(D)}$ ) and resonance fluorescence upon donor excitation (black circles;  $F_{542(D)}$ ) displayed inverted changes, whereas acceptor

fluorescence (filled triangles;  $F_{542(A)}$ ) stayed largely constant (Fig. 1 C, bottom). These configurations ensured the FRET reduction and low level of quenching of sensor proteins during the recordings. Kinetics of  $FR$  reduction ( $\tau_{FR}$ ) and the minimum amount of  $FR$  ( $FR_{min}$ ) under the receptor stimulation were obtained by fitting to the FRET data with a single-exponential decay function (Fig. 1 C, middle).

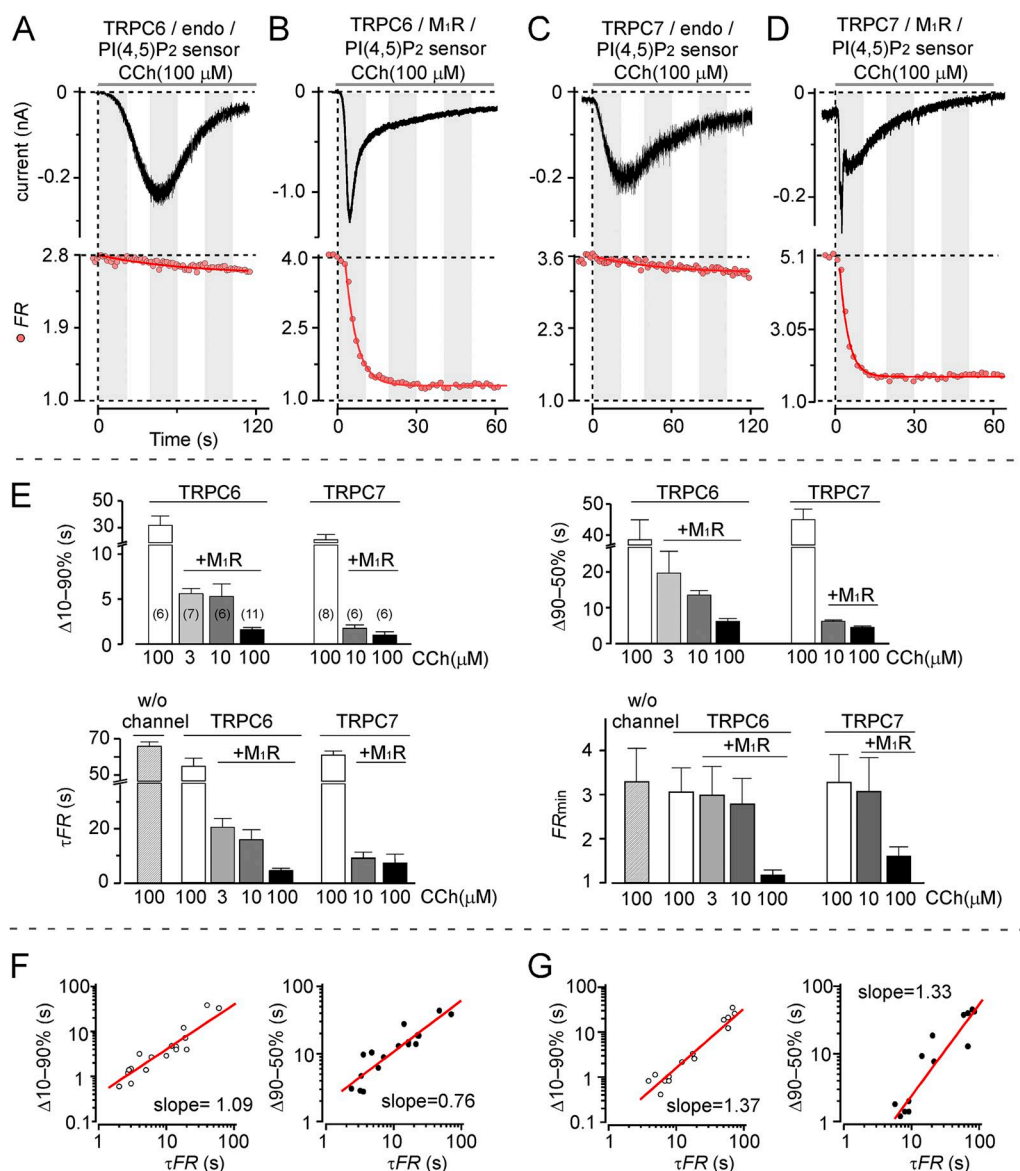


**Figure 2.** Correlation between the TRPC6/7 currents and the decay of PI(4,5)P<sub>2</sub>. (A and B) Example traces of TRPC6 currents (top) and FRET of PI(4,5)P<sub>2</sub> sensor (CFP<sub>msec</sub>-PHd and YFP<sub>msec</sub>-PHd) (bottom) upon stimulation with 100 μM CCh of either endogenous (A) or overexpressed M<sub>1</sub>R (B). (C and D) Same as in A and B, but in cells expressing TRPC7. (E) Summary of currents and FRET changes. TRPC6/7 current increase (Δ10-90%) and decay (Δ90-50%), kinetics of FRET reduction ( $\tau_{FR}$ ), and degree of FRET reduction ( $FR_{min}$ ) were accelerated in a CCh concentration and M<sub>1</sub>R expression-dependent manner. The data depicted by the stripe and the white bars show without channel expression (transfected only PI(4,5)P<sub>2</sub> sensor) and endogenous receptor stimulation, respectively. Numbers in parentheses indicate the number of cells measured, here and throughout. (F and G) Time courses of the Δ10-90% and Δ90-50% of receptor-operated currents were plotted against the simultaneously measured  $\tau_{FR}$  (F, TRPC6; G, TRPC7). These data were obtained from various concentrations of CCh or level of M<sub>1</sub>R expression. The slope with a linear fit highlights a relationship between the time courses and  $\tau_{FR}$ .

### PI(4,5)P<sub>2</sub> dynamics at different levels of receptor stimulation and TRPC6/7 currents

We then explored the effect of PI(4,5)P<sub>2</sub> reduction on TRPC6 or TRPC7 channel currents at varying levels of receptor stimulation. Stimulation of endogenous muscarinic receptors in HEK293 cells with 100 μM CCh evoked prolonged TRPC6 current and a small amount of reduction in *FR* (Fig. 2 A). The time for TRPC6 current activation ( $\Delta 10\text{--}90\%$ ) and inactivation ( $\Delta 90\text{--}50\%$ ) were  $32 \pm 7$  s and  $39.2 \pm 6.7$  s ( $n = 6$ ), respectively. In accordance with the current time course,  $\tau FR$  was lengthened to  $55.3 \pm 4.5$  s, and  $FR_{\min}$  stayed near the resting level. Reduction in *FR* was only  $18 \pm 6\%$ . Previous studies have shown that depletion of PI(4,5)P<sub>2</sub> can be induced by overexpression of M<sub>1</sub>R (Xie et al., 2011; Dickson et al., 2013). Consistent with these studies, overexpressing M<sub>1</sub>R and treating the cells with a high concentration of CCh (100 μM) greatly accelerated the TRPC6 current and FRET reduction (Fig. 2 B) ( $\Delta 10\text{--}90\% = 1.6 \pm 0.3$  s;  $\Delta 90\text{--}50\% = 6.2 \pm 0.9$  s;  $\tau FR = 4.5 \pm 0.9$  s), and enhanced

the *FR* reduction with a near zero FRET efficiency ( $FR_{\min} = 1.15 \pm 0.1$  and  $E_{\text{EFF}} = 0.016 \pm 0.01$ ;  $n = 11$ ). Intriguingly, the time to reach the peak current was remarkably shortened compared with endogenous muscarinic receptor stimulation at the same concentration of CCh (100 μM; +M<sub>1</sub>R =  $2.8 \pm 0.7$  s; endo =  $63 \pm 8$  s). Similar tendencies in the *FR* reduction and the peak time were observed when TRPC7 was expressed instead of TRPC6, except for the shorter activation and inactivation time for TRPC7 current (Fig. 2, C and D). In addition, TRPC7's  $\tau FR$  was slightly delayed and  $FR_{\min}$  was also slightly attenuated compared with that of TRPC6. (Data from the different strength of receptor stimulation was summarized in Fig. 2 E.)

To elucidate the functionality of PI(4,5)P<sub>2</sub> hydrolysis, we focused on the kinetic relationships between TRPC6/7 currents and FRET reduction. For that purpose, the log-log plots for the activation or the inactivation of TRPC6/7 currents and the values of  $\tau FR$  were made using data obtained at varying levels of agonist stimulation, with and

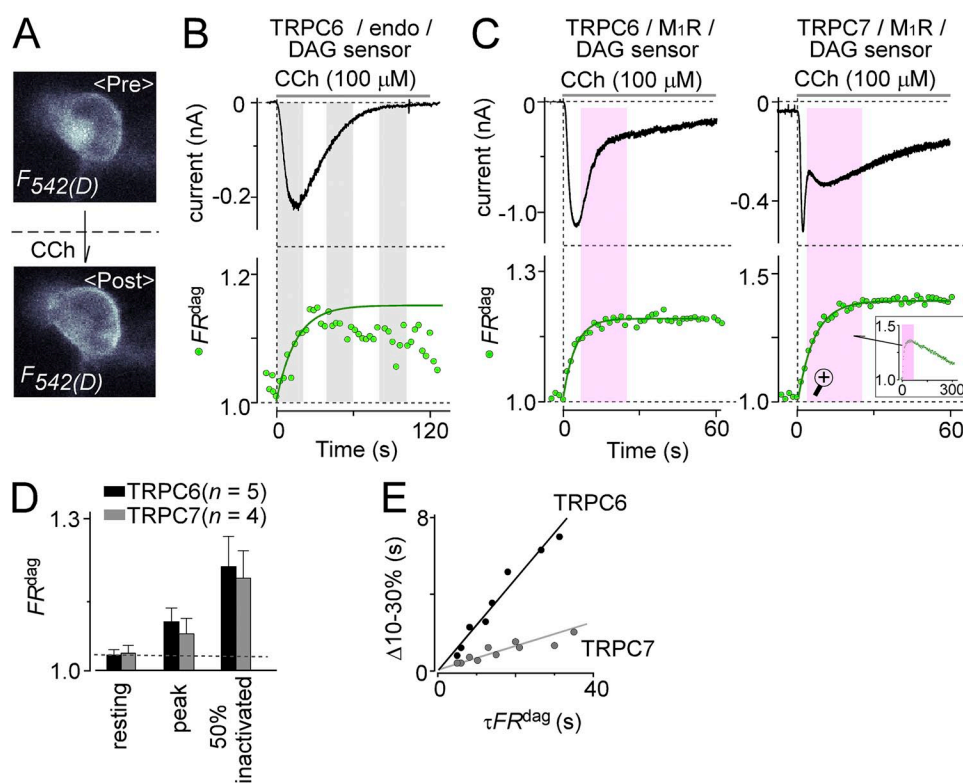


**Figure 3.** Incompatible correlation between receptor-operated TRPC6/7 currents and DAG production. (A) Principle of DAG detection by PKC probe FRET. Increments in FRET caused by the translocation of PKC $\epsilon$ -CFP<sub>msec</sub> to the plasma membrane were detected by a coexpressed membrane-resident acceptor protein (Mry-YFP<sub>msec</sub>) in HEK293 cells. (B) Whole-cell TRPC6 currents (top) and FRET changes caused by DAG increments, “*FR*<sup>dag</sup>” (bottom, green circles), recorded from endogenous muscarinic receptor stimulation with 100 μM CCh. The rise of FRET was fitted to the exponential equation:  $FR^{\text{dag}} = FR_{\text{max}}^{\text{dag}} - \Delta FR^{\text{dag}} \times \exp(-t / \tau FR^{\text{dag}})$  (green solid curve). (C) Traces of currents and *FR*<sup>dag</sup> in M<sub>1</sub>R-overexpressing cells with 100 μM CCh. (Left) TRPC6 currents. (Right) TRPC7 currents. Prolonged DAG production was observed. Purple zones indicate inconsistencies between current inactivation and DAG production. The inset in the TRPC7 panel shows *FR*<sup>dag</sup> changes over a longer time scale (300 s). (D) Summary of *FR*<sup>dag</sup> levels at the respective current points observed in the robust receptor stimulation (+M<sub>1</sub>R and 100 μM). The black and gray bars denote expression of TRPC6 and TRPC7 channels, respectively. (E) Time courses of initial phase of current increase ( $\Delta 10\text{--}30\%$ ) were plotted against kinetics of DAG production ( $\tau FR^{\text{dag}}$ ).

without M<sub>1</sub>R overexpression (Fig. 2, F and G). These log–log plots showed a clear correlation between  $\tau FR$  and the current time courses ( $\Delta 10$ –90% [left panels] and  $\Delta 90$ –50% [right panels]) for both TRPC6 and TRPC7 currents. The linear relationship that appeared in a plot of the relation of  $\Delta 90$ –50% to  $\tau FR$  in TRPC7-expressing cells showed significantly steeper slopes (slope = 1.33) than that in TRPC6-expressing cells (slope = 0.76) (Fig. 2, F and G). This steepness may reflect higher TRPC7 sensitivity to reduction in PI(4,5)P<sub>2</sub> than TRPC3 or TRPC6 (Imai et al., 2012). In addition to the FRET decay, the extent of the reduction or depletion of PI(4,5)P<sub>2</sub> levels ( $FR_{\min}$ ) also showed a similar tendency to the time course of current activation or inactivation of each channel (Fig. S1). These plots, however, were slightly more scattered than those of  $\tau FR$ . Such a scattering was probably caused by cell-to-cell variability in the released IP<sub>3</sub> in response to the hydrolysis of PI(4,5)P<sub>2</sub> (Irvine and Schell, 2001). The simultaneous detection of PI(4,5)P<sub>2</sub> and TRPC currents demonstrated that the activation and inactivation time courses related to both the kinetics and the extent of PI(4,5)P<sub>2</sub> reduction.

#### Simultaneous detection of DAG and receptor-operated TRPC channel current

TRPC3/6/7 channels are DAG-sensitive ion channels, but the manner in which DAG dynamics correlate with these TRP channels' activity remains largely unknown. To address this question, DAG production was concurrently monitored with receptor-operated TRPC6/7 channel currents. The detection of DAG dynamics relies on membrane translocation of DAG-activated PKC in response to increasing DAG levels at the plasma membrane (Violin et al., 2003) (Fig. 3 A). We used Ca<sup>2+</sup>-insensitive PKC $\epsilon$  as a fluorescence donor molecule to exclude Ca<sup>2+</sup>-dependent translocation of PKC (Sinnecker and Schaefer, 2004). Upon stimulation with CCh through the endogenous muscarinic receptors, TRPC6 current and DAG production were initiated almost simultaneously (Fig. 3 B). This parallel response is consistent with TRPC6 being a DAG-sensitive channel. Furthermore, during the inactivation of the TRPC6 channel current, DAG level also declined. This synchronicity indicated that when the strength of receptor stimulation was weak, the production of DAG levels seemed to be a critical factor to the current appearances.

Contrary to the synchronicity of the TRPC6 current and DAG dynamics in the weak receptor stimulation, when the cells overexpressed M<sub>1</sub>R, the simultaneous measurement was revealed to be inconsistent. The activation of TRPC6 channel current paralleled DAG production, whereas the inactivation of the channel did not; there was no decline in DAG production (Fig. 3 C, left, purple zone). This lack of temporal consistency between the current decay and DAG levels was even more prominent in the TRPC7 channel, which exhibited

inactivation while DAG levels were still increasing (Fig. 3 C, right, and summarized in D). This inconsistency may be explained by the idea that PKC-mediated phosphorylation inhibits channel opening, which has been proposed for TRPC3 (Soboloff et al., 2007).

However, for TRPC6 channel, there was no significant difference in the current inactivation ( $\Delta 90$ –50%) between cells overexpressing PKC $\epsilon$  (TRPC6, M<sub>1</sub>R, and DAG sensor-expressing,  $7.5 \pm 2.5$  s;  $n = 5$ ) and control (TRPC6 and M<sub>1</sub>R,  $6.2 \pm 0.9$  s;  $n = 11$ ). In addition, a previous report has shown that PKC $\delta$  exerts a negative feedback effect via phosphorylation of Ser448 of TRPC6 (Bousquet et al., 2010). Using the phosphorylation-insensitive mutant TRPC6<sup>S448A</sup> and its corresponding mutant TRPC7<sup>S394A</sup>, we tested whether the PKC-mediated phosphorylation of these residues is involved in the current decay. Under the robust receptor stimulation, unexpectedly, we did not detect any clear difference in the  $\Delta 90$ –50% time (100  $\mu$ M CCh: TRPC6<sup>wt</sup>,  $11.4 \pm 2.4$  s; TRPC6<sup>S448A</sup>,  $12.7 \pm 2.7$  s; TRPC7<sup>wt</sup>,  $1.8 \pm 1.1$  s; TRPC7<sup>S394A</sup>,  $1.9 \pm 0.9$  s;  $n = 8$ ). Furthermore, the basal phosphorylation site of TRPC6 has been identified at Ser<sup>814</sup> (Bousquet et al., 2011), which may play a role in the channel function. We also tested the mutant, TRPC6<sup>S814A</sup>, but it failed to show any significant differences, including  $\Delta 90$ –50% ( $10.1 \pm 3.5$  s;  $n = 7$ ), which is consistent with the previous report (Bousquet et al., 2011). Our data do not exclude the possibility that PKC-mediated phosphorylation inhibits channel opening, because of the variety of cell and measurement conditions. Nevertheless, these results suggest that the DAG production level and PKC phosphorylation-mediated channel modulation may contribute less to the inactivation of TRPC6/7 channels at the robust stimulation.

A simulation model was built for further understanding of dual regulation by PI(4,5)P<sub>2</sub> and DAG, as described in the latter section. For that purpose, we presented the relation between the current increase and the production of DAG. Plotting the early phase of the current increase ( $\Delta 10$ –30%) versus DAG production kinetics ( $\tau FR^{\text{lag}}$ ) exhibited a clear correlation, with a smaller slope for the TRPC7 compared with the TRPC6-expressing cells (Fig. 3 E). This result suggests that the TRPC7 channel is highly sensitive to the increment of DAG. We thus set the DAG sensitiveness in the initial parameter as TRPC7 > TRPC6 in the model simulation (Table 4, rows 21 and 22).

#### Functional dissociation constants of PI(4,5)P<sub>2</sub> binding to TRPC3/6/7 channels

These results have shown the substantial importance of the dissociation of PI(4,5)P<sub>2</sub> to the inactivation of TRPC6/7 channel currents, but the affinity of PI(4,5)P<sub>2</sub> to these channels is not yet known. To obtain this parameter, DrVSP, which functions as a membrane-resident voltage-controllable phosphoinositides phosphatase, was

used to reduce intrinsic PI(4,5)P<sub>2</sub> (Okamura et al., 2009). Our previous report demonstrated that reduction of PI(4,5)P<sub>2</sub> by activation of DrVSP led to concomitant inhibition of TRPC3/6/7 currents (Imai et al., 2012). We simultaneously measured the voltage-dependent stepwise controls of FRET between CFP<sub>msec</sub>-PHd and YFP<sub>msec</sub>-PHd, and the DrVSP-mediated inhibition. To evoke the currents, the DAG lipase inhibitor, RHC80267, was used. This compound is suitable to produce stabilized inward currents, mainly caused by elevating the resting level of DAG (Albert et al., 2005). The step-pulse protocol, from 20 to 180 mV with a duration of 500 ms, enables the current inhibition and FRET reduction to be observed simultaneously (Fig. 4 A).

By plotting the current inhibition “ $r(I)$ ” and FRET reduction “ $r(FR)$ ” against the depolarizing pulses that activate DrVSP, the various sensitivities of the TRPC3, TRPC6, and TRPC7 channels were quantified (Fig. 4 B). The inhibition of the TRPC3 current (Fig. 4 B, left, circles) was relatively insensitive, compared with the reduction in FRET (triangles). In contrast, the inhibition of TRPC7 was highly sensitive to the reduction in FRET (Fig. 4 B, right). TRPC6 exhibited a similar level of gradual changes in  $r(I)$  and  $r(FR)$  (Fig. 4 B, middle). This result confirms our previous observations showing differential sensitivities of TRPC3/6/7 channels to PI(4,5)P<sub>2</sub> reduction, with an order of TRPC7 > C6 > C3 (Imai et al., 2012).

However, the inhibition of TRPC3 and TRPC6 currents was not complete, and the FRET reduction by DrVSP

activation was also insufficient to reach a zero FRET level ( $FR = 1.46 \pm 0.07$ ;  $n = 14$  at 120 mV). We thus speculated that this partial current inhibition may simply be because of the incomplete depletion of PI(4,5)P<sub>2</sub>. This idea raises a challenging question: how is TRPC3/6/7 inhibition by DrVSP activation observed at the single-channel level? To answer this question, DrVSP was activated during receptor stimulation in the cell-attached patch mode. Robust depolarization led to a brief, but almost complete, inhibition of the TRPC6 channel during the bursting activity (Fig. S2). This observation enabled us to use a standard ligand-binding isotherm for PI(4,5)P<sub>2</sub>-TRPC3/6/7 channel binding. The calculation of PI(4,5)P<sub>2</sub> concentration from the reduction in  $FR$  was done by a boundary function (described in Materials and methods). Because the FRET between CFP<sub>msec</sub>-PHd and YFP<sub>msec</sub>-PHd proteins is cancelled by detachment of either the donor or acceptor fluorophore-fused PHd proteins from the membrane,  $FR$  reduction could be approximated as a cooperative square law of the membrane-bound fraction of PHD (Eq. 3) as follows:

$$\frac{FR}{FR_{max}} \approx F^2 = \left( 1 / \left( 1 + \frac{K_{d(PHD)}}{[PI(4,5)P_2]} \right) \right)^2, \quad (4)$$

where  $K_{d(PHD)}$  is the dissociation constant of PI(4,5)P<sub>2</sub> binding to the PHD. The left side of Eq. 4 is always positive, and solving PI(4,5)P<sub>2</sub> yields:

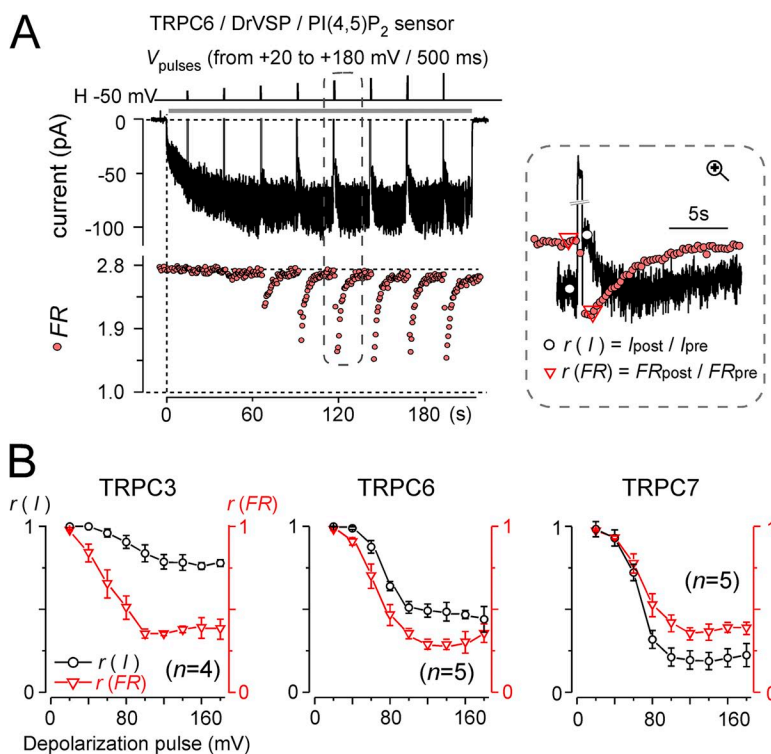


**Figure 4.** TRPC current inhibition and PI(4,5)P<sub>2</sub> reduction in response to the protocol for measuring the voltage dependence of DrVSP activation. (A) TRPC6, CFP<sub>msec</sub>-PHd, YFP<sub>msec</sub>-PHd (PI(4,5)P<sub>2</sub> sensor), and voltage-sensing phosphatase (DrVSP) were coexpressed in HEK293 cells. Gradual current inhibition and reduction in PI(4,5)P<sub>2</sub> caused by the step-pulse protocol (left; from 20 to 180 mV; duration of 500 ms; repeated every 25 s). A DAG lipase inhibitor (RHC80267; 100 μM) was applied to induce the currents (gray horizontal bar). The ratio of current inhibition,  $r(I)$ , and FRET reduction,  $r(FR)$ , upon the depolarization pulses was used to quantify the channel activity and PI(4,5)P<sub>2</sub> changes after DrVSP activation (right). (B) The voltage dependence of current inhibition (left axis; circles) and  $FR$  reduction (right axis; triangles) after DrVSP activation in cells expressing TRPC3 (left), TRPC6 (middle), and TRPC7 (right) channels.

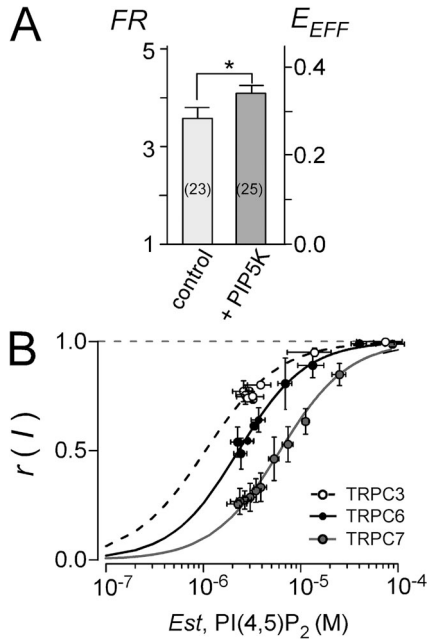


**Figure 5.** Functional dissociation constants of PI(4,5)P<sub>2</sub> binding to TRPC3/6/7 channels. (A) Comparison of  $FR$  or  $E_{EFF}$  in the resting condition between cells expressing TRPC6 channel and CFP<sub>msec</sub>-PHd and YFP<sub>msec</sub>-PHd (control), and those overexpressing PIP5K (+PIP5K). The  $FR$  of cells overexpressing PIP5K increased on average by  $\sim 1.2$ -fold compared with control cells. \*,  $P < 0.05$ ; unpaired  $t$  test. (B) Steady-state plots for estimating the functional  $K_d$  of PI(4,5)P<sub>2</sub> binding to TRPC3/6/7 channels. Horizontal axis indicates the estimated PI(4,5)P<sub>2</sub> concentration based on the conversion from  $FR$  to PI(4,5)P<sub>2</sub>, according to Eq. 5.

$$Est, [PI(4,5)P_2] = K_{d(PHd)} \cdot \sqrt{\frac{FR}{FR_{max}}} - \left(1 - \sqrt{\frac{FR}{FR_{max}}}\right), \quad (5)$$

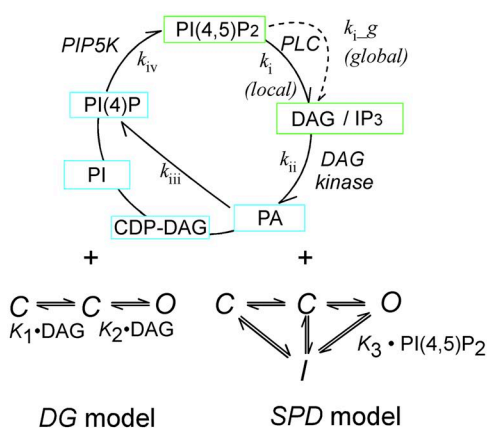
where  $FR_{max}$  is the maximum  $FR$  value at an infinite concentration of PI(4,5)P<sub>2</sub>. According to the resting  $FR$  of PIP5K-overexpressing cells, that value was estimated as 1.2-fold higher than the resting  $FR$  of the control cells (Fig. 5 A). After solving Eq. 5,  $r(I)$  versus the estimated PI(4,5)P<sub>2</sub> concentration (*Est*, PI(4,5)P<sub>2</sub>) plots were fitted using the Hill equation (Hill, 1910) (Fig. 5 B). Assuming a dissociation constant of PI(4,5)P<sub>2</sub> – PHd = 2  $\mu$ M (Hirose et al., 1999), the functional dissociation constants of PI(4,5)P<sub>2</sub> binding to TRPC3, TRPC6, and TRPC7 channels were estimated at 1, 2, and 5  $\mu$ M, respectively. These factors were incorporated into  $K_3$  as the initial parameter for simulation in channel regulation by PI(4,5)P<sub>2</sub> (see below).

### Modeling TRPC channel activity coupled to PI(4,5)P<sub>2</sub>-DAG signaling

Having determined the functional constants of PI(4,5)P<sub>2</sub> binding to TRPC channels, we attempted to simulate channel activity and compare the results with the experimental data. Our model consists of three components. Part 1 covers the minimal PI(4,5)P<sub>2</sub>-to-DAG reaction, including the process of PI(4,5)P<sub>2</sub> recovery (Table 1, Eqs. 6–17). Part 2 is the calculation of the open probability ( $P_o$ ) and the resultant current based on the dynamics of DAG and PI(4,5)P<sub>2</sub> concentrations (Table 2, Eqs. 18–20). Part 3 is a back-calculation of normalized  $FR$  of PI(4,5)P<sub>2</sub> sensor according to the concentrations of PI(4,5)P<sub>2</sub> and IP<sub>3</sub> (Table 3; Eqs. 21–26). Details of the respective components are described in full below.

(Part 1) Scheme of the minimum essential PI(4,5)P<sub>2</sub>-DAG reaction. The goals of this simulation were to reproduce

### A PI(4,5)P<sub>2</sub> – DAG reaction scheme



### B DG vs SPD

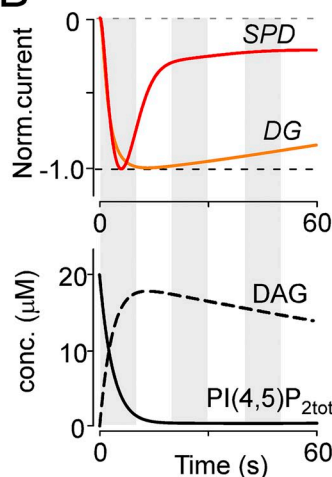


**Figure 6.** PI(4,5)P<sub>2</sub> reaction model and channel gating models (DG and SPD) used for simulations. (A) Minimal PI(4,5)P<sub>2</sub>-DAG reaction scheme (top). Hydrolysis of PI(4,5)P<sub>2</sub> (local) is the first step in this model ( $k_i$ ). The produced DAG can serve as a substrate for DAG kinase, DAG lipase, and DAG acetyltransferase. For simplicity, we refer only to DAG kinase ( $k_{ii}$ ). PA, phosphatidic acid. Further catalytic steps for the producing of CDP-DAG and PI were bound to directly generate PI(4)P ( $k_{iii}$ ). The PI(4,5)P<sub>2</sub> recovery from PI(4)P by PIP5K is referred to as “ $k_{iv}$ ”. PI(4,5)P<sub>2</sub> and DAG concentrations are linked to the three-state DG (bottom left) and the four-state SPD (bottom right) models. (B) Comparison of TRPC6 current data processed through the DG and SPD simulation models with parameters of the accelerated PLC kinetics. The top panel shows that a rapid decay of TRPC6 current was seen with the SPD model (red trace), but not with the DG model (orange trace). The current amplitudes were normalized to their peak currents (Norm.current). The bottom panel shows the simulated dynamics of PI(4,5)P<sub>2</sub> (solid line) and DAG (dashed line) concentrations.

the experimental data and elucidate the functional role of the reduction in PI(4,5)P<sub>2</sub> caused by agonist-induced receptor-operated currents. Thus, we focused on the activation of PLC by G<sub>q</sub> protein-coupled receptors as follows. The initial step is hydrolysis of PI(4,5)P<sub>2</sub> by PLC, which generates DAG and IP<sub>3</sub> (Fig. 6 A,  $k_i$ , and Table 1, Eqs. 6–8). Activation of PLC starts at the first time step (0.05 s) after time zero. In the factor of PLC activity, we also included the adjusted factors of receptor desensitization (Table 1, Eq. 9) and the time-dependent acceleration of PLC activity by receptor stimulation (Eq. 10). The latter factor has been demonstrated as Ca<sup>2+</sup>-dependent positive feedback in PLC activity (Horowitz et al., 2005). The next step is DAG phosphorylation by DAG kinase to generate phosphatidic acid (PA) (Fig. 6 A,  $k_{ii}$ , and Table 1, Eq. 11). The third step is production of PI(4)P, a precursor of PI(4,5)P<sub>2</sub>, from PA, skipping the intermediate

products of CDP-DAG and phosphatidylinositol (Fig. 6 A,  $k_{iii}$ , and Table 1, Eq. 12). For recovery of PI(4,5)P<sub>2</sub>, we considered two pathways: (1) resynthesis of PI(4,5)P<sub>2</sub> from PI(4)P by PIP5K (Fig. 6 A,  $k_{iv}$ , and Table 1, Eq. 13) and (2) diffusion of PI(4,5)P<sub>2</sub> from global to local channel area (Eqs. 14 and 15). The idea and necessity of the diffusion pathway are described in the Discussion and the legend of Fig. S4. The amount of scavenged PI(4,5)P<sub>2</sub> arising from the binding of PHd proteins was solved by Eq. 16 (Table 1). The total available amount of PI(4,5)P<sub>2</sub> to transfer to Part 2 (channel gating) was calculated by Eq. 17 (Table 1).

*(Part 2) Channel gating.* Two channel gating models were constructed. The first, a simple channel gating model, only consists of DAG binding and unbinding for channel opening and closing, and it lacks the inhibitory regulation

TABLE 1  
Equations for minimal PI(4,5)P<sub>2</sub>-DAG reaction scheme

Equation	No.
$d[\text{PI}(4,5)\text{P}_2]_{\text{local}} = d[\text{PI}(4,5)\text{P}_2]_{\text{local}} - d[\text{PI}(4,5)\text{P}_2]_{\text{local}} \cdot k_{i(t)} \cdot \text{De}_{f(t)} \cdot dt$	6
$d[\text{DAG}] = d[\text{DAG}] + d[\text{PI}(4,5)\text{P}_2]_{\text{tot}} \cdot k_{i(t)} \cdot \text{De}_{f(t)} \cdot dt - d[\text{DAG}] \cdot k_{ii} \cdot dt$	7
$d[\text{IP}_3] = d[\text{IP}_3] + d[\text{PI}(4,5)\text{P}_2]_{\text{tot}} \cdot k_{i(t)} \cdot \text{De}_{f(t)} \cdot dt - d[\text{IP}_3] \cdot k_v \cdot dt$	8
$\text{De}_{f(t)} = 1 - (\text{Rd}_f \cdot \exp(-\tau_{rd}/t) + \text{Sd}_f \cdot \exp(-\tau_{sd}/t))$ Rd <sub>f</sub> : fraction of rapid desensitization Sd <sub>f</sub> : fraction of slow desensitization τ <sub>rd</sub> : time constant for the rapid desensitization τ <sub>sd</sub> : time constant for the slow desensitization	9
$k_{i(t)} = k_i \cdot \text{B\_PLC}^{\text{pg}}$ B <sub>PLC</sub> : basal PLC activity pg : power parameter of G <sub>q</sub> PCR receptor stimulation	10
$d[\text{PA}] = d[\text{PA}] + d[\text{DAG}] \cdot k_{ii} \cdot dt - d[\text{PA}] \cdot k_{iii} \cdot dt$	11
$d[\text{PI}(4)\text{P}] = d[\text{PI}(4)\text{P}] + d[\text{PA}] \cdot k_{iii} \cdot dt - d[\text{PI}(4)\text{P}] \cdot k_{iv} \cdot dt$	12
$d[\text{PI}(4,5)\text{P}_2]_{\text{recovered}} = d[\text{PI}(4)\text{P}] \cdot k_{iv} \cdot dt - d[\text{PI}(4,5)\text{P}_2]_{\text{recovered}} \cdot k_{i(t)} \cdot \text{De}_{f(t)} \cdot dt$	13
$d[\text{PI}(4,5)\text{P}_2]_{\text{global}} = d[\text{PI}(4,5)\text{P}_2]_{\text{global}} - d[\text{PI}(4,5)\text{P}_2]_{\text{global}} \cdot k_{i_g(t)} \cdot \text{De}_{f(t)} \cdot dt$ $k_{i_g}$ : rate constant for global PLC activity	14
$d[\text{PI}(4,5)\text{P}_2]_{\text{diffused\_in}} = (d[\text{PI}(4,5)\text{P}_2]_{\text{global}} - d[\text{PI}(4,5)\text{P}_2]_{\text{local}}) \cdot (1 - \text{erff}(\text{spot} / \text{sprt}(4 \cdot \text{dcoef} \cdot dt))) - d[\text{PI}(4,5)\text{P}_2]_{\text{diffused\_in}} \cdot k_{i(t)} \cdot \text{De}_{f(t)} \cdot dt$ erff : error function dcoef : diffusion coefficient of PI(4,5)P <sub>2</sub> spot : distance between local and global domain	15
$d[\text{PI}(4,5)\text{P}_2]_{\text{scavenged\_PHd}} = (d[\text{PHd}]_{\text{rel}} - d[\text{PHd}]_{\text{IP}_3}) \cdot (1 / (1 + \text{K}_{d,\text{PHd}} / (d[\text{PI}(4,5)\text{P}_2]_{\text{local}} + d[\text{PI}(4,5)\text{P}_2]_{\text{recovered}} + d[\text{PI}(4,5)\text{P}_2]_{\text{diffused\_in}})))$	16
$d[\text{PI}(4,5)\text{P}_2]_{\text{tot}} = d[\text{PI}(4,5)\text{P}_2]_{\text{local}} + d[\text{PI}(4,5)\text{P}_2]_{\text{recovered}} + d[\text{PI}(4,5)\text{P}_2]_{\text{diffused\_in}} - d[\text{PI}(4,5)\text{P}_2]_{\text{scavenged\_PHd}}$	17

TABLE 2  
Equations for channel gating

Comment to the equation	Equation	No.
Open probability in DG model:	$P_o = (K_1 \cdot K_2 / d[\text{DAG}]^2 + K_2 / d[\text{DAG}] + 1)^{-1}$	18
Open probability in SPD model:	$P_o = \left[ \frac{K_1 \cdot K_2 / d[\text{DAG}]^2 + K_2 / d[\text{DAG}] + (K_1 \cdot K_2 / d[\text{DAG}]^2) \cdot (K_3 / d[\text{PI}(4,5)\text{P}_2]_{\text{tot}})}{+K_2 \cdot (K_3 / d[\text{PI}(4,5)\text{P}_2]_{\text{tot}}) / d[\text{DAG}] + (K_3 / d[\text{PI}(4,5)\text{P}_2]_{\text{tot}}) + 1} \right]^{-1}$ <p><math>K_1</math> and <math>K_2</math> are dissociation constants for DAG to TRPC channel.  <math>K_3</math> is dissociation constant for PI(4,5)P<sub>2</sub> to TRPC channel.</p>	19
TRPC6 / C7 currents:	$I = N \cdot g \cdot P_o \cdot (V_h - V_{rev})$ <p><math>N</math> : number of channels  <math>g</math> : single channel conductance  <math>V_h</math> : holding potential (-50 mV)  <math>V_{rev}</math> : reversal potential (0 mV)</p>	20

by PI(4,5)P<sub>2</sub> reduction (termed the ‘‘DG model’’ in Fig. 6 A, bottom left). The second is a realistic model that takes into account the inhibitory effect caused by a reduction of PI(4,5)P<sub>2</sub> that directly induces transition of the channel to an inactive state from any closed or open state. This model is referred to as the ‘‘SPD model’’ (Fig. 6 A, bottom right). Open probabilities ( $P_o$ ) expressed as a function of agonist concentration, calculated according to the DG and SPD models, are described in Eqs. 18 and 19, respectively (Table 2). Finally, whole-cell currents were calculated using Eq. 20.

(Part 3) Back-calculation of  $FR$  from the simulated PI(4,5)P<sub>2</sub> concentration. As described in the previous section, the observed  $FR$  changes were converted to PI(4,5)P<sub>2</sub> concentrations, according to Eq. 5. Here, we attempted to do the opposite, using these equations to explore FRET dynamics. Receptor stimulation produces DAG and IP<sub>3</sub> after PLC-mediated hydrolysis of PI(4,5)P<sub>2</sub>. IP<sub>3</sub> is highly

diffusible in the cytoplasm and binds to PHd proteins with higher affinity (0.1 μM) than PI(4,5)P<sub>2</sub> (Hirose et al., 1999). The factor of FRET reduction caused by the binding of IP<sub>3</sub> to PI(4,5)P<sub>2</sub> sensor was incorporated into the back-calculation of  $FR$  dynamics (Table 3, Eqs. 21–24). Although it was difficult to calculate the absolute efficiency of FRET, because of various expression levels of fluorophore-fused PHd, we could estimate the normalized  $FR$  (Norm. $FR$ ) changes by the resting level of  $FR$ . The alternations in Norm. $FR$ , caused by CFP<sub>msec</sub>-fused TRPC7 channel versus YFP<sub>msec</sub>-PHd and CFP<sub>msec</sub>-PHd versus YFP<sub>msec</sub>-PHd, were solved by Eqs. 25 and 26 (Table 3), respectively.

#### Insufficient matching of the DG model

First, we examined whether a model without PI(4,5)P<sub>2</sub> regulation (DG model) was able to reproduce the experimental data of the simultaneous measurements. Fitting to the TRPC6 currents was accomplished by minimizing the sum of the squared errors with 19 free parameters,

TABLE 3  
Equations for the back-calculated  $FR$

Comment to the equation	Equation	No.
Fraction of IP <sub>3</sub> bound PHd (PHd):	$d(\text{PHd}_{\text{IP3b}}) = 1 - d[\text{PHd}]_{\text{IP3}} / [\text{PHd}]_{\text{tot}}$	21
Concentration of membrane bound PHd:	$d[\text{PHd}]_{\text{rem}} = [\text{PHd}]_{\text{tot}} - d[\text{PHd}]_{\text{rel}}$	22
Concentration of cytosolic PHd upon PI(4,5)P <sub>2</sub> reduction:	$d[\text{PHd}]_{\text{rel}} = (1 - 1 / (K_{d,\text{PHd}} / d[\text{PI}(4,5)\text{P}_2]_{\text{tot}} + 1)) \cdot [\text{PHd}]_{\text{tot}}$	23
Concentration of IP <sub>3</sub> bound PHd:	$d[\text{PHd}]_{\text{IP3}} = (1 / (K_{d,\text{IP3}} / d[\text{IP}_3] + 1)) \cdot d[\text{PHd}]_{\text{rel}}$	24
Norm. $FR$ between TRPC7-CFP <sub>msec</sub> and YFP <sub>msec</sub> -PHd:	$\text{Norm.}FR = d(\text{PHd}_{\text{IP3b}}) \cdot \left( \frac{1}{1 + K_{d,\text{PHd}} / d[\text{PI}(4,5)\text{P}_2]_{\text{tot}}} \right) \cdot \left[ \frac{1}{1 + K_{d,\text{PHd}} / [\text{PI}(4,5)\text{P}_2]_{\text{tot}(0)}} \right]^{-1}$ <p style="text-align: center;"><math>[\text{PI}(4,5)\text{P}_2]_{\text{tot}(0)}</math> : PI(4,5)P<sub>2</sub> concentration at time zero</p>	25
Norm. $FR$ between CFP <sub>msec</sub> -PHd and YFP <sub>msec</sub> -PHd:	$\text{Norm.}FR = d(\text{PHd}_{\text{IP3b}}) \cdot \left( \frac{1}{1 + K_{d,\text{PHd}} / d[\text{PI}(4,5)\text{P}_2]_{\text{tot}}} \right)^2 \cdot \left[ \frac{1}{1 + K_{d,\text{PHd}} / [\text{PI}(4,5)\text{P}_2]_{\text{tot}(0)}} \right]^{-1}$	26

the initial values of which are listed in Table 4. The fidelity of the model was assessed by a similarity of *FR* between the experimentally measured *FR* and simulated *FR*, which was obtained from the back-calculation of the resultant PI(4,5)P<sub>2</sub> concentrations by fitting to the currents, according to the equations described in the section on model Part 3 and Table 3.

When the currents were induced by the weak receptor stimulation through endogenous muscarinic receptors, the experimental *FR* was substantially compatible with the calculated *FR* from the simulated PI(4,5)P<sub>2</sub> changes (Fig. S4 A; SD = 0.12). In contrast, fitting the currents in M<sub>1</sub>R-overexpressing cells to the DG model highly deviated from the experimental *FR* changes (Fig. S4 B; SD = 0.63). Furthermore, the DAG production was quite more transient than that observed in the PKC-based FRET dynamics (Fig. S4 B, bottom panel, dashed line). Therefore our fitting examination indicates that the DG model may be useful for mimicking

the delayed receptor-operated currents, but it is not totally suitable for the rapid case. As we demonstrated, when the parameter for PLC activity ( $k_i$ ) was set to an accelerated kinetics ( $k_i = 0.7$ ), a marked TRPC6 current inactivation emerged only in the SPD model but not in the DG model (Fig. 6 B, top).

#### Fitting the SPD model to the experimental data

The SPD model was then tested. The same basic fitting strategy as in the DG model was used. After fitting the SPD model to the experimental receptor-operated current data, the computed PI(4,5)P<sub>2</sub> data were compared with the experimental *FR* dynamics. In this case, in addition to the 19 parameters, the dissociation constant of PI(4,5)P<sub>2</sub> binding was incorporated at  $K_3$  (Table 4, row 23). The fitting of the SPD model to the whole-cell TRPC6 currents did indeed show overlapping of the dynamics of the experimental Norm.*FR* and the back-calculated Norm.*FR*, with a smaller SD value than in the

TABLE 4  
*Parameters and initial conditions for the fitting*

Row	Parameters (unit)	Setting	Initial value of TRPC6 endo/C6 + M <sub>1</sub> R/A7r5/C7 + M <sub>1</sub> R	Source or comments
1	PI(4,5)P <sub>2</sub> (μM) at resting	Free	20/20/20/20	Bunce et al., 1993; McLaughlin and Murray, 2005
2	$k_i$ _PLC (s <sup>-1</sup> )	Free	0.04/1/1/1	Rational to PI(4,5)P <sub>2</sub> reduction with our data
3	$k_{ii}$ _DAG kinase (s <sup>-1</sup> )	Free	0.03/0.03/0.08/0.03	Rational to DAG changes with our data
4	$k_{iii}$ _PA to PIP reactions (s <sup>-1</sup> )	Free	0.01/0.01/0.01/0.01	Appropriate for PI(4,5)P <sub>2</sub> synthesis
5	$k_{iv}$ _PIP5K (s <sup>-1</sup> )	Free	0.1/0.1/0.25/0.1	Appropriate for PI(4,5)P <sub>2</sub> resynthesis
6	$k_v$ _IP <sub>3</sub> phosphatase (s <sup>-1</sup> )	Free	0.5/0.5/0.5/0.5	Appropriate for IP <sub>3</sub> hydrolysis
7	$\tau_{rid}$ (s)	Free	5/2/1/4	Appropriate for Receptor desensitization
8	$\tau_{sid}$ (s)	Free	50/10/5/10	Same as above
9	Rd_f (no unit)	Free	0.5/0.5/0.5/0.5	Same as above
10	Sd_f (no unit)	Free	0.5/0.5/0.5/0.5	Same as above
11	spot (distance global to local; μm)	Free	4/4/3/4	5 times more than the diffusion coefficient of PI(4,5)P <sub>2</sub>
12	dcoef of PI(4,5)P <sub>2</sub> (μm <sup>2</sup> /s)	Free	0.8/0.8/0.8/0.8	Golebiewska et al., 2008
13	Ratio of local $k_i$ / global $k_i$	Free	1/4/2/5	Approximate from the uneven FRET reduction (Fig. S3)
14	PI4P (μM)	Fixed	10/10/10/10	Brown et al., 2008
15	Activation delay (no unit)	Free	0.01/0.001/0.001/0.001	Appropriate for receptor activation
16	Activation power (no unit)	Free	0.5/0.3/0.7/0.3	Same as above
17	Vrev (mV)	Fixed	0/0/0/0	
18	Vhold (mV)	Fixed	-50/-50/-50/-50	
19	No. of channels	Free	100-7,000	Appropriate for the current density
20	Channel conductance (pS)	Fixed	35/35/35/70	Hofmann et al., 1999; Lemonnier et al., 2008
21	$K_1$ ( $K_d$ for DAG1; μM)	Free	60/60/35/10	Effective OAG concentrations are 10 to 100 μM in Hofmann et al., 1999; Okada et al., 1999; Imai et al., 2012
22	$K_2$ ( $K_d$ for DAG2; μM)	Free	30/30/10/10	Same as above
23	$K_3$ ( $K_d$ for PI(4,5)P <sub>2</sub> ; μM)	Free	2/2/5/5	This paper, Fig. 4 D
24	Expressed PHd (μM)	Fixed	1.6/1.6/1.6/1.6	This paper, Materials and methods
25	$K_d$ PI(4,5)P <sub>2</sub> of PHd (μM)	Fixed	2.0/2.0/2.0/2.0	Hirose et al., 1999
26	$K_d$ IP <sub>3</sub> of PHd (μM)	Fixed	0.1/0.1/0.1/0.1	Hirose et al., 1999

DG model ( $SD = 0.04$ ;  $n = 4$ ). Furthermore, similar overlapping was clearly evident in TRPC6 currents in M<sub>1</sub>R-overexpressing cells ( $SD = 0.05$ ;  $n = 4$ ; Fig. 7 B, middle). The fitting expressed a prolonged existence of DAG, persisting well beyond the current decay (Fig. 7 B, bottom, solid dashed line). Such prolonged existence of DAG was seen experimentally after robust receptor stimulation (Fig. 3 B) and in recent work by Falkenburger et al. (2013). The correlation between the experimental and modeled data supports the description of TRPC6 currents and PI(4,5)P<sub>2</sub> dynamics in the SPD model (fitted parameters are summarized in Table 5).

The SPD model was also examined for TRPC6/7-like currents in aortic smooth muscle-derived A7r5 cells (Brueggemann et al., 2006; Maruyama et al., 2006). The PI(4,5)P<sub>2</sub> sensor proteins (CFP<sub>msec</sub>-PHd and YFP<sub>msec</sub>-PHd) were coexpressed in A7r5 cells without exogenous expression of channels or receptors (Fig. 7 C, inset). By applying AVP, TRPC6/7-like currents and FRET reduction were observed similarly to the observations after stimulation of HEK293 cells with CCh (Fig. 7 C, top and middle). A noticeable difference was that PI(4,5)P<sub>2</sub> recovered quickly (5–20 s after the application of AVP).

Such rapid FRET recovery is expected with the rapid desensitization of vasopressin receptors, and was reproduced by coexpressing vasopressin type 1A receptors with TRPC6 or TRPC7 channel in HEK293 cells (Fig. S5). When fitting these AVP-evoked TRPC6/7-like currents, the simulation parameters for rapid desensitization (Table 4, rows 7 and 8) also overlapped the Norm.FR dynamics (Fig. 7 C, middle, blue line;  $SD = 0.12$ ). These results indicate that the SPD model is useful even in the context of physiological cells.

Contrary to these positive results, the back-calculated FRET demonstrated less similarity to the experimental FRET achieved by fitting to TRPC7 currents observed in HEK293 cells and vice versa (Fig. S6;  $SD = 0.18$ ;  $n = 4$ ). In addition, TRPC7 currents often demonstrated a plateau or biphasic response when M<sub>1</sub>R was overexpressed, but the FRET did not clearly show such irregular dynamics. We reasoned that the FRET detection by fluorophore-fused PHd was too slow to respond to the PI(4,5)P<sub>2</sub> dynamics compared with the time course of TRPC7 current, recorded by the electrophysiological method. To improve this issue, we redesigned the FRET pairs to detect PI(4,5)P<sub>2</sub> changes in the local vicinity of the TRPC7

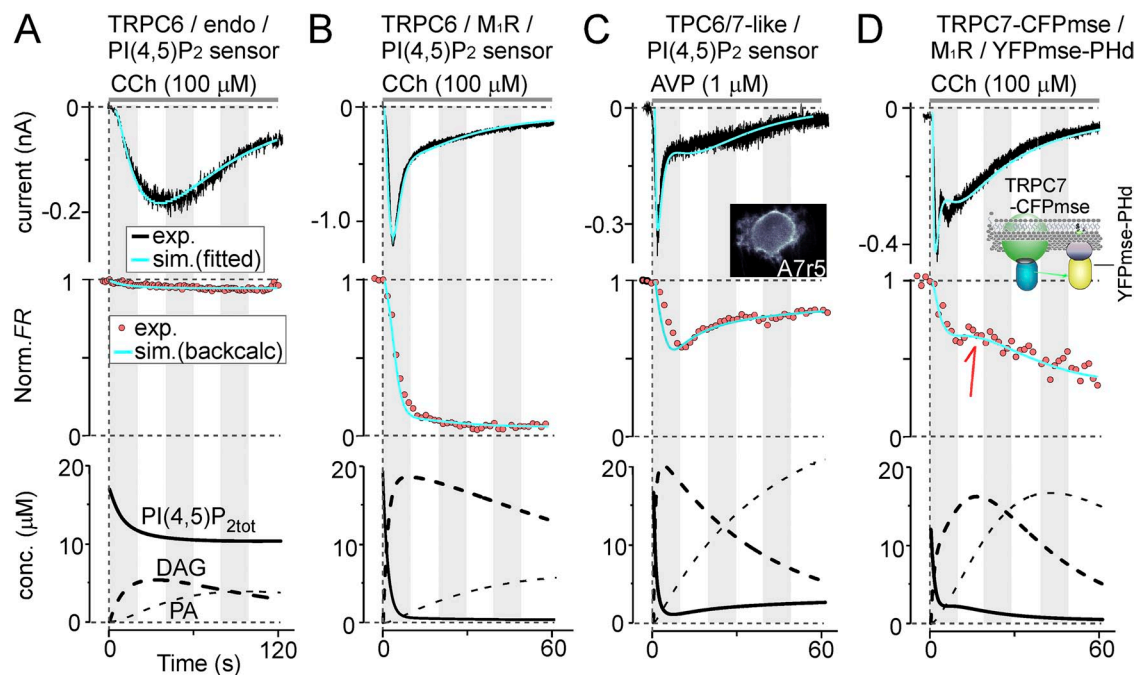


**Figure 7.** SPD model fitting to experimentally observed TRPC6/7 currents and AVP-evoked TRPC6/7-like currents in A7r5 cells. (A) Fitting of the receptor-operated TRPC6 current simultaneously measured with PI(4,5)P<sub>2</sub> by FRET with the SPD model (top; light blue trace). The experimental data were obtained from the low strength of receptor stimulation carried by CCh application (100 μM) to endogenous muscarinic receptor in HEK293 cells. Back-calculated FR of PI(4,5)P<sub>2</sub> concentrations at the respective points (bottom; solid) was normalized against the time zero FR (Norm.FR; middle; light blue), and that was overlaid on the experimental Norm.FR (middle; circles). The bottom panel displays the fitting resultant changes in PI(4,5)P<sub>2</sub> (solid), DAG (dashed), and PA (thin dashed). The similarity of Norm.FR was assessed by SD as described in Materials and methods. (B) Fitting of experimental TRPC6 current data from M<sub>1</sub>R-overexpressing cells. The initial parameters are identical to those in A. (C) Fitting of experimental TRPC6/7-like currents recorded from A7r5 aorta-derived smooth muscle cells. The currents were evoked by 1 μM AVP. The inset in the top panel shows A7r5 cells expressing the PI(4,5)P<sub>2</sub> sensor. (D) Fitting of TRPC7 currents. Local PI(4,5)P<sub>2</sub> dynamics were detected using a FRET donor linked to the TRPC7 channel at the end of its C-terminal domain (top; inset). Transient increments in FRET were detected during the plateau or biphasic response (middle; arrow).

channels. The donor fluorophore (CFP<sub>mse</sub>) directly fused to the channel was coexpressed with YFP<sub>mse</sub>-PHd (Fig. 7 D, inset). Intriguingly, this FRET pair showed a transient increment of FRET during the plateau or biphasic current (Fig. 7 D, red arrow). By fitting the TRPC7 currents with the corresponding “down-up-down” PI(4,5)P<sub>2</sub> dynamics (Fig. 7 D, bottom), we achieved an improved matching of Norm.FR (SD = 0.14) as well. This transient up-regulation of PI(4,5)P<sub>2</sub> reflects a quick replenishment by diffusible PI(4,5)P<sub>2</sub> in the SPD model (Fig. S3). These results show that corresponding Norm.FR responses in various cell and channel settings strongly support the fidelity of the SPD model for reproducing simultaneous events of receptor-operated TRPC currents and FR changes.

## DISCUSSION

Because PI(4,5)P<sub>2</sub> hydrolysis by PLC is the critical event in receptor-operated TRPC3/6/7 currents, the parallel observation of PI(4,5)P<sub>2</sub> or DAG with channel activity is fundamental to advancing our understanding of channel regulation. To address this point, we performed concerted quantitative FRET measurements of sensitized

fluorescence emission (3-cube method) and electrophysiological measurements on patch-clamped cells. We accomplished this by using CFP<sub>mse</sub>- or YFP<sub>mse</sub>-fused PHd proteins as a FRET sensor of PI(4,5)P<sub>2</sub>, or CFP<sub>mse</sub>-fused PKC $\epsilon$  and YFP<sub>mse</sub>-fused myristoyl membrane-attached peptides to monitor DAG. CCh or AVP was used to induce TRPC6/7 currents, which were measured to monitor the synchronicity of receptor-operated currents and changes in either PI(4,5)P<sub>2</sub> or DAG levels. The experimental results demonstrated a correlation between the kinetics of PI(4,5)P<sub>2</sub> reduction and the activation or the inactivation of receptor-operated TRPC6/7 currents. Fitting the experimental data to the DG or SPD model revealed that the idea of self-limiting regulation by PI(4,5)P<sub>2</sub> and DAG is critical for reproducing receptor-operated TRPC6/7 currents.

### Reproducing the currents and FRET reduction in the SPD model

Our results show that reduction in PI(4,5)P<sub>2</sub> by PLC-mediated hydrolysis appears to be fundamental to the inactivation of TRPC6/7 channels. This contribution is even more apparent after robust receptor stimulation, either by high concentrations of receptor agonist or by

TABLE 5  
Resultant parameters by fitting to TRPC currents with SPD model

Cell	HEK293	HEK293	A7r5	HEK293	
Transfected plasmids	TRPC6/CFPmse-PHd/ YFPmse-PHd	TRPC6/M <sub>1</sub> R/CFPmse- PHd/YFPmse-PHd	CFPmse-PHd/YFPmse- PHd	TRPC7-CFPmse/M <sub>1</sub> R/ YFPmse-PHd	
Receptor agonist (conc. $\mu$ M)	CCh (100)	CCh (100)	Arg-Vasopressin (1)	CCh (100)	
The number of fitted cells	4	4	4	4	
Row	Parameters (unit)				
1	PI(4,5)P <sub>2</sub> ( $\mu$ M) at resting	22.5 $\pm$ 0.4	23.0 $\pm$ 0.4	22.2 $\pm$ 0.2	14.6 $\pm$ 0.1
2	$k_{i\_PLC}$ ( $s^{-1}$ )	0.05 $\pm$ 0.02	1.2 $\pm$ 0.20	1.3 $\pm$ 0.42	0.93 $\pm$ 0.09
3	$k_{ii\_DAG}$ kinase ( $s^{-1}$ )	0.04 $\pm$ 0.01	0.03 $\pm$ 0.02	0.07 $\pm$ 0.03	0.02 $\pm$ 0.01
4	$k_{iii\_PA}$ to PIP reactions, ( $s^{-1}$ )	0.008 $\pm$ 0.002	0.006 $\pm$ 0.002	0.004 $\pm$ 0.001	0.006 $\pm$ 0.0001
5	$k_{iv\_PIP5K}$ ( $s^{-1}$ )	0.050 $\pm$ 0.004	0.07 $\pm$ 0.04	0.17 $\pm$ 0.083	0.04 $\pm$ 0.03
6	$k_{v\_IP_3}$ phosphatase ( $s^{-1}$ )	0.7 $\pm$ 0.4	0.2 $\pm$ 0.1	0.88 $\pm$ 0.093	0.84 $\pm$ 0.14
7	$\tau_{rd}$ (s)	12.0 $\pm$ 3.8	1.4 $\pm$ 0.6	1.4 $\pm$ 0.2	4.4 $\pm$ 0.4
8	$\tau_{sd}$ (s)	24 $\pm$ 11	17 $\pm$ 5.2	6 $\pm$ 2.4	38 $\pm$ 15
9	Rd_f (no unit)	0.65 $\pm$ 0.08	0.55 $\pm$ 0.03	0.60 $\pm$ 0.12	0.46 $\pm$ 0.05
10	Sd_f (no unit)	0.35 $\pm$ 0.05	0.44 $\pm$ 0.02	0.43 $\pm$ 0.124	0.53 $\pm$ 0.06
11	spot (distance global to local; $\mu$ m)	0.64 $\pm$ 0.09	2.78 $\pm$ 0.79	2.83 $\pm$ 0.98	1.90 $\pm$ 0.29
12	dcoef of PI(4,5)P <sub>2</sub> ( $\mu$ m <sup>2</sup> /s)	0.36 $\pm$ 0.08	0.8 $\pm$ 0.47	0.5 $\pm$ 0.11	0.29 $\pm$ 0.06
13	Ratio of local $k_i$ / global $k_i$	1.1 $\pm$ 0.28	4.0 $\pm$ 1.6	2.8 $\pm$ 0.98	6.0 $\pm$ 1.3
14	Activation delay factor	0.03 $\pm$ 0.024	0.01 $\pm$ 0.002	0.003 $\pm$ 0.002	0.03 $\pm$ 0.025
15	Activation power factor	0.6 $\pm$ 0.33	0.32 $\pm$ 0.07	0.7 $\pm$ 0.17	0.3 $\pm$ 0.12
16	The number of channels	1,644 $\pm$ 277	5,808 $\pm$ 959	317 $\pm$ 121	2,384 $\pm$ 1,896
17	$K_1$ ( $k_d$ for DAG1; $\mu$ M)	39 $\pm$ 6.3	26 $\pm$ 2.4	23 $\pm$ 7.6	7.0 $\pm$ 0.3
18	$K_2$ ( $k_d$ for DAG2; $\mu$ M)	29 $\pm$ 5.1	22 $\pm$ 2.0	8 $\pm$ 3.4	6.3 $\pm$ 0.25
19	$K_3$ ( $k_d$ for PI(4,5)P <sub>2</sub> ; $\mu$ M)	1.9 $\pm$ 0.6	3.0 $\pm$ 0.66	9 $\pm$ 1.5	9.7 $\pm$ 0.14
	SD	0.04	0.05	0.12	0.14
	$Sr_{0.01}$ <sup>a</sup>	82.7%	80.9%	70.1%	56.2%

Parameters are presented as mean  $\pm$  SEM. (Typical results are displayed in Fig. 7.)

<sup>a</sup>Percentage of the squared residuals lower than the value of 0.01.

overexpression of functional receptors. Here, we simulate in a virtual setting the inhibitory role played by a reduction in PI(4,5)P<sub>2</sub> levels in the SPD model in the context of different levels of PLC activity. In the averaged fitted data for TRPC6 currents, PLC activity ( $k_i$ ) was gradually decreased or increased, as shown in Fig. 8 A. The simulated TRPC6 currents and FRET by the PHd clearly demonstrated PLC-dependent dynamics in regard to the amplitudes or kinetics in the currents (Fig. 8 A, top) and the kinetics or the extent of FRET reduction (bottom). We then depicted log-log plots of the time course of current growth ( $\Delta 10-90\%$ ) or decay ( $\Delta 90-50\%$ ) versus  $\tau_{FR}$  (Fig. 8 B, red circles). For comparison, we also simulated this plot with the DG model (Fig. 8 B, black circles) as well as TRPC7 channels. The log-log plots of  $\Delta 10-90\%$  to  $\tau_{FR}$  showed a linear relationship in both SPD and DG models of TRPC6/7 currents. These plots closely resemble the experimental data, which are shown as gray lines in Fig. 8 B (solid and dashed line for TRPC6 and TRPC7 channels, respectively). In contrast, the linear relationship between current decay ( $\Delta 90-50\%$ ) and  $\tau_{FR}$  was reproduced only when modeled with the SPD model (Fig. 8 B, right, red symbols), but not with the DG model.

The simulation result indicates that when the strength of receptor stimulation PI(4,5)P<sub>2</sub> is low or the reduction of PI(4,5)P<sub>2</sub> is delayed ( $\tau_{FR} > 50$  s), the DG model may be useful to reproduce such delayed receptor-operated TRPC currents. However, the situation alters as receptor stimulation is strengthened or the reduction of PI(4,5)P<sub>2</sub> is accelerated, and the DG model deviates from the

experimental data. Furthermore, the SPD model-based relationship in  $\Delta 90-50\%$  TRPC7 currents to  $\tau_{FR}$  resulted in a slight increase in the steepness to TRPC6 (Fig. 8 B). This result is similar to the TRPC7 current to  $\tau_{FR}$  relationship observed experimentally (Fig. 8 B, dotted line). In contrast, the SPD model-based TRPC6 relationship resulted in an even steeper slope compared with the experimentally observed relationship (Fig. 8 B, solid line). The difference implies further unknown characteristics that underlie the regulation by PI(4,5)P<sub>2</sub> and DAG in receptor-operated TRPC6/7 currents. Recently, several reports have addressed an alternation of PI(4,5)P<sub>2</sub> regulation by intracellular Ca<sup>2+</sup> in KCNQ2/3 (Kosenko et al., 2012; Falkenburger et al., 2013) and TRPV6 channels (Cao et al., 2013). According to Kosenko et al. (2012), calmodulin binding to KCNQ2 channels stabilized PI(4,5)P<sub>2</sub> channel binding. The involvement of Ca<sup>2+</sup> regulation to PI(4,5)P<sub>2</sub> or DAG regulations requires further investigation. Nevertheless, because of the consistency of the SPD model simulation with the experimental results, we concluded that the inhibitory effect of reductions in PI(4,5)P<sub>2</sub> would accelerate the channel inactivation with the increased receptor stimulation.

#### Proposed function of the self-limiting regulation in receptor-operated TRPC6/7 currents

Based on the model simulation, we explored several PLC-dependent features of the self-limiting regulation by PI(4,5)P<sub>2</sub> and DAG. The first characteristic is the maximum  $P_o$  ( $P_{o,max}$ ). As shown in the left plot in Fig. 8 C, in both models,  $P_{o,max}$  values gradually increased as PLC

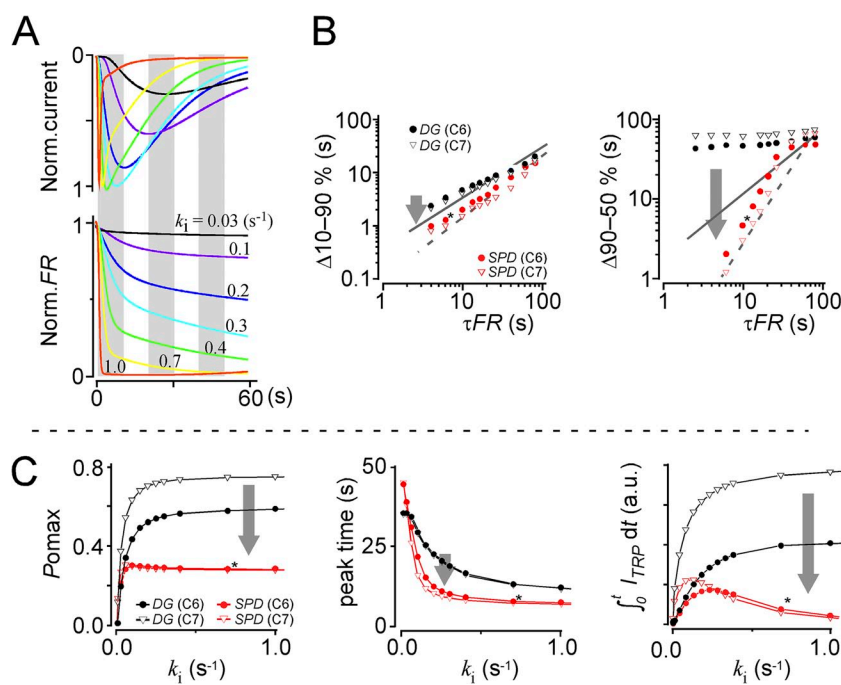


**Figure 8.** Proposed contribution of PI(4,5)P<sub>2</sub> reduction in receptor-operated TRPC6/7 currents. (A) Representative SPD model simulations for receptor-operated TRPC6 currents (top) and FRET by PI(4,5)P<sub>2</sub> sensor (bottom) from various PLC activities ( $k_i$ ).  $k_i$  varied from 0.03 to 1.0 (s<sup>-1</sup>). The same color curves displayed in each panel were calculated from the same  $k_i$  value. (B) The various kinetics of PI(4,5)P<sub>2</sub> reduction ( $\tau_{FR}$ ) according to the changes in PLC activity ( $k_i$ ) impact activation (left;  $\Delta 10-90\%$ ) and inactivation (right;  $\Delta 90-50\%$ ) of TRPC6/7 channel currents. Shown are the prediction made by the DG model (black) and the SPD model (red) for TRPC6 (circles) and TRPC7 channels (triangles). The star in the panels indicates the result from the  $k_i$  setting of 0.7. The solid and dashed lines indicate the current- $\tau_{FR}$  relationships experimentally observed in TRPC6 and TRPC7, respectively. The direction of the arrows and its size indicate the gap from the DG to SPD model. (C) Simulation results of PLC-dependent characteristics of TRPC6/7 channels by DG (black) and SPD (red) models. (Left) The relationship between maximum open probability ( $P_{o,max}$ ) and  $k_i$ . (Middle) The time required to peak currents (s) and  $k_i$ . (Right) The total ionic influx and  $k_i$ .  $t = 30$  s.

activity increased in the range where the  $k_i$  values were small ( $k_i$  of  $<0.1$ ). However,  $P_{\text{omax}}$  in the SPD model was sustained or slightly attenuated when the  $k_i$  values were  $>0.1$ . Kwon et al. (2007) showed that disruption of the potential PI(4,5)P<sub>2</sub>-sensing residue of the TRPC6 channel nearly doubles the maximum current amplitude. This is consistent with our simulation, where the  $P_{\text{omax}}$  at  $k_i = 0.7 \text{ s}^{-1}$  eventually increased by two- to threefold in the DG model compared with that in the SPD model. The consistency of our simulation and the previous report strongly supports the functionality of the self-limiting regulation in TRPC6/7 channels for protecting the excess cation influx.

The second characteristic we measured was the shift in peak appearance. When we applied robust receptor stimulation, the time to peak currents were drastically shortened compared with the endogenous receptor stimulation (see PI(4,5)P<sub>2</sub> dynamics at different levels... in Results). Essentially, the similar tendency was reproduced in both models (Fig. 8 C, middle). However, the time to peak shortening was even more striking in the SPD model (Fig. 8 C, red symbols) than in the DG model (black symbols). Petersson et al. (2011) computationally demonstrated that TRPC channel activity in the nervous system contributes to the temporal integration of the generation of a lower rate-firing pattern at distal dendrites. Their simulation result suggests that the rate of firing may be controlled by the peak time of TRPC currents. Therefore, TRPC6/7 channels may play a critical role in determining the neural firing rate, depending on the strength of receptor stimulation.

The third characteristic is the total ionic influx relation (Fig. 8 C, right). The total ionic influx, which was calculated by integration of the flow during the receptor stimulation ( $t = 30 \text{ s}$ ), was predicted as the bell-shape response to the PLC activity in the SPD model. Therefore, the optimum PLC activity appeared neither weak nor robust, but was in the middle ( $0.1 < k_i < 0.3$ ; Fig. 8 C, right, red symbols). TRPC3/6/7 channels contribute to vascular tone, inflammation, cell remodeling, and intestinal contraction through increased Na<sup>+</sup> or Ca<sup>2+</sup> levels (Tsvilovsky et al., 2009; Smedlund et al., 2010; Tauseef et al., 2012; Weissmann et al., 2012; Koenig et al., 2013). Hence, this bell-shaped relationship may be linked to these multiple pathophysiological responses.

Collectively, channel inhibition by PI(4,5)P<sub>2</sub> reduction in DAG-sensitive TRPC3/6/7 channels not only accelerates the rate of current decay but also contributes to suppression of the current amplitude, shortening of the peak time, and the bell shape of the ionic influx, leading to the multiple functionality of these channels.

#### PI(4,5)P<sub>2</sub> replenishment mechanism by diffusion

It has been suggested that phosphatidylinositol 4-phosphate is critical for replenishing PI(4,5)P<sub>2</sub> via its phosphorylation by PIP5K (Suh and Hille, 2002; Loew, 2007).

Furthermore, PIP5K substantially contributes to the quick recovery of PI(4,5)P<sub>2</sub> after its depletion by DrVSP activation (Falkenburger et al., 2010; Imai et al., 2012). However, in case of receptor-operated TRPC6/7 currents, we observed that a high concentration of ATP or its inactive analogue AMP-PNP in the patch-pipette solution had little effect on TRPC6/7 currents (Fig. S7), even in the plateau or biphasic phase. We speculate that an additional PI(4,5)P<sub>2</sub> replenishment pathway, such as the detachment of PI(4,5)P<sub>2</sub> from proteins, dispersion from its clustered complex (van den Bogaart et al., 2011), translocation of phosphoinositides from the PIS organelle (Kim et al., 2011), or an unknown mechanism (Hammond et al., 2012), may be involved.

However, here we focused on the lateral diffusion of PI(4,5)P<sub>2</sub>. When we analyzed FRET in regions of small compartments, a nonuniform reduction in *FR* by PI(4,5)P<sub>2</sub> sensor upon receptor stimulation was observed (Fig. S3). This variability of a region-specific PI(4,5)P<sub>2</sub> reduction was consistent with an electron microscopic study showing that PI(4,5)P<sub>2</sub> located in a membrane microdomain (known as caveolae) decreased slower than in an undifferentiated membrane upon receptor stimulation (Fujita et al., 2009). We have speculated that such nonuniformity of PI(4,5)P<sub>2</sub> reduction creates the opportunity for PI(4,5)P<sub>2</sub> diffusion to occur. For that reason, we incorporated the pathway of PI(4,5)P<sub>2</sub> replenishment by lateral diffusion into our model (Part 1). By incorporation of this pathway, the plateau or biphasic currents after the peak current can be enhanced as the gap of PI(4,5)P<sub>2</sub> dynamics between the local and global domain increases (Fig. S3). In the case of TRP channels in flies, the plateau phase of the TRP current in response to light adaptation has been demonstrated to have a key role in phototransduction (Lo and Pak, 1981; Minke, 2010). Therefore, incorporation of replenishment of PI(4,5)P<sub>2</sub> in our model may provide an important contribution to understanding the physiological consequences.

#### Molecular insight into PI(4,5)P<sub>2</sub> and DAG binding to TRPC channels

The fitting result of the SPD model predicted the dissociation constant of DAG binding to TRPC6 channel to be 20 to  $\sim 40 \mu\text{M}$  and to TRPC7 to be  $<10 \mu\text{M}$  (Table 5, rows 17 and 18). This parameter has not been well characterized, despite being critical for DAG-sensitive TRPC channel activation. In the experiment, receptor-operated TRPC7 currents demonstrated a higher sensitivity to DAG production (Fig. 3 E) than TRPC6 currents, which was consistent with the result predicted by the SPD model, thus providing a fundamental parameter into the TRPC6/7 channel activation. However, it is still unclear exactly where these lipids bind to the TRPC3/6/7 channels.

Among the TRP superfamily, heat- and capsaicin-activated TRPV channels are relatively well characterized

and have at least two PI(4,5)P<sub>2</sub>-binding sites in the C-terminal domains, proximal and distal regions to the S6 domain (Prescott and Julius, 2003; Doerner et al., 2011; Ufret-Vincenty, et al., 2011). In the case of the TRPC family, earlier studies have also shown that the distal region of the TRPC6 C-terminal domain contributes to the current decay (Kwon et al., 2007), whereas PI(4,5)P<sub>2</sub> binding to the PH-like domain in the N-terminal region reduces TRPC3 current amplitudes (van Rossum et al., 2005). These results indicate that PI(4,5)P<sub>2</sub> binding may be supported by multiple channel domains/regions in a complex manner. Furthermore, another complex point regarding the PI(4,5)P<sub>2</sub> regulation is that various heteromeric TRPC3/6/7 channels can be formed, including heteromers of TRPC3/6/7 (Goel et al., 2002) and other subfamilies (Hofmann et al., 2002; Takai et al., 2004; Ambudkar et al., 2006). Addressing these points is essential to further extend our understanding on the self-limiting regulation by PI(4,5)P<sub>2</sub> and DAG signals observed in TRPC3/6/7 channels.

We thank Masato Hirata (Kyushu University), Michael Schaefer (Leipzig University), and Moritoshi Sato (The university of Tokyo) for their helpful advice on the detection of PI(4,5)P<sub>2</sub> and DAG. We thank to Yasuo Mori and Nozomi Ogawa (Kyoto University) for the critical reading of our manuscript. Miho Sumiyoshi (Fukuoka University) assisted with the molecular biological preparations.

This work was supported by Grants-in-Aid for Young Scientists from the Japan Society for the Promotion of Sciences and the Naito Foundation (both to M.X. Mori).

The authors declare no competing financial interests.

Author contributions: K. Itsuki and M.X. Mori conceived the study. K. Itsuki, H. Hase, and M.X. Mori performed the experiments and analyzed the data. Y. Okamura and R. Inoue provided guidance and support throughout. K. Itsuki, Y. Imai, Y. Okamura, R. Inoue, and M.X. Mori wrote the paper.

Sharona E. Gordon served as editor.

Submitted: 17 May 2013

Accepted: 8 January 2014

## REFERENCES

Albert, A.P., A.S. Piper, and W.A. Large. 2005. Role of phospholipase D and diacylglycerol in activating constitutive TRPC-like cation channels in rabbit ear artery myocytes. *J. Physiol.* 566:769–780. <http://dx.doi.org/10.1113/jphysiol.2005.090852>

Ambudkar, I.S., B.C. Bandyopadhyay, X. Liu, T.P. Lockwich, B. Paria, and H.L. Ong. 2006. Functional organization of TRPC-Ca<sup>2+</sup> channels and regulation of calcium microdomains. *Cell Calcium.* 40:495–504. <http://dx.doi.org/10.1016/j.ceca.2006.08.011>

Beech, D.J., K. Muraki, and R. Flemming. 2004. Non-selective cationic channels of smooth muscle and the mammalian homologues of *Drosophila* TRP. *J. Physiol.* 559:685–706. <http://dx.doi.org/10.1113/jphysiol.2004.068734>

Bousquet, S.M., M. Monet, and G. Boulay. 2010. Protein kinase C-dependent phosphorylation of transient receptor potential canonical 6 (TRPC6) on serine 448 causes channel inhibition. *J. Biol. Chem.* 285:40534–40543. <http://dx.doi.org/10.1074/jbc.M110.160051>

Bousquet, S.M., M. Monet, and G. Boulay. 2011. The serine 814 of TRPC6 is phosphorylated under unstimulated conditions. *PLoS ONE.* 6:e18121. <http://dx.doi.org/10.1371/journal.pone.0018121>

Brandt, B.L., B.W. Kimes, and F.G. Klier. 1976. Development of a clonal myogenic cell line with unusual biochemical properties. *J. Cell. Physiol.* 88:255–275. <http://dx.doi.org/10.1002/jcp.1040880302>

Brown, S.A., F. Morgan, J. Watras, and L.M. Loew. 2008. Analysis of phosphatidylinositol-4,5-bisphosphate signaling in cerebellar Purkinje spines. *Biophys. J.* 95:1795–1812. <http://dx.doi.org/10.1529/biophysj.108.130195>

Brueggemann, L.I., D.R. Markun, K.K. Henderson, L.L. Cribbs, and K.L. Byron. 2006. Pharmacological and electrophysiological characterization of store-operated currents and capacitative Ca<sup>2+</sup> entry in vascular smooth muscle cells. *J. Pharmacol. Exp. Ther.* 317:488–499. <http://dx.doi.org/10.1124/jpet.105.095067>

Bunce, C.M., P.J. French, P. Allen, J.C. Mountford, B. Moor, M.F. Greaves, R.H. Michell, and G. Brown. 1993. Comparison of the levels of inositol metabolites in transformed haemopoietic cells and their normal counterparts. *Biochem. J.* 289:667–673.

Cao, C., E. Zakharian, I. Borbiri, and T. Rohacs. 2013. Interplay between calmodulin and phosphatidylinositol 4,5-bisphosphate in Ca<sup>2+</sup>-induced inactivation of transient receptor potential vanilloid 6 channels. *J. Biol. Chem.* 288:5278–5290. <http://dx.doi.org/10.1074/jbc.M112.409482>

Dickson, E.J., B.H. Falkenburger, and B. Hille. 2013. Quantitative properties and receptor reserve of the IP<sub>3</sub> and calcium branch of G<sub>q</sub>-coupled receptor signaling. *J. Gen. Physiol.* 141:521–535. <http://dx.doi.org/10.1085/jgp.201210886>

Doerner, J.F., H. Hatt, and I.S. Ramsey. 2011. Voltage- and temperature-dependent activation of TRPV3 channels is potentiated by receptor-mediated PI(4,5)P<sub>2</sub> hydrolysis. *J. Gen. Physiol.* 137:271–288. <http://dx.doi.org/10.1085/jgp.200910388>

Erickson, M.G., B.A. Alseikhan, B.Z. Peterson, and D.T. Yue. 2001. Preassociation of calmodulin with voltage-gated Ca<sup>2+</sup> channels revealed by FRET in single living cells. *Neuron.* 31:973–985. [http://dx.doi.org/10.1016/S0896-6273\(01\)00438-X](http://dx.doi.org/10.1016/S0896-6273(01)00438-X)

Falkenburger, B.H., J.B. Jensen, and B. Hille. 2010. Kinetics of PIP<sub>2</sub> metabolism and KCNQ2/3 channel regulation studied with a voltage-sensitive phosphatase in living cells. *J. Gen. Physiol.* 135:99–114. <http://dx.doi.org/10.1085/jgp.200910345>

Falkenburger, B.H., E.J. Dickson, and B. Hille. 2013. Quantitative properties and receptor reserve of the DAG and PKC branch of G<sub>q</sub>-coupled receptor signaling. *J. Gen. Physiol.* 141:537–555. <http://dx.doi.org/10.1085/jgp.201210887>

Firth, A.L., C.V. Remillard, and J.X. Yuan. 2007. TRP channels in hypertension. *Biochim. Biophys. Acta.* 1772:895–906. <http://dx.doi.org/10.1016/j.bbadis.2007.02.009>

Fujita, A., J. Cheng, K. Tauchi-Sato, T. Takenawa, and T. Fujimoto. 2009. A distinct pool of phosphatidylinositol 4,5-bisphosphate in caveolae revealed by a nanoscale labeling technique. *Proc. Natl. Acad. Sci. USA.* 106:9256–9261.

Gamper, N., and M.S. Shapiro. 2007. Regulation of ion transport proteins by membrane phosphoinositides. *Nat. Rev. Neurosci.* 8:921–934. <http://dx.doi.org/10.1038/nrn2257>

Goel, M., W.G. Sinkins, and W.P. Schilling. 2002. Selective association of TRPC channel subunits in rat brain synaptosomes. *J. Biol. Chem.* 277:48303–48310. <http://dx.doi.org/10.1074/jbc.M207882200>

Golebiewska, U., M. Nyako, W. Woturski, I. Zaitseva, and S. McLaughlin. 2008. Diffusion coefficient of fluorescent phosphatidylinositol 4,5-bisphosphate in the plasma membrane of cells. *Mol. Biol. Cell.* 19:1663–1669. <http://dx.doi.org/10.1091/mbc.E07-12-1208>

Hammond, G.R., M.J. Fischer, K.E. Anderson, J. Holdich, A. Koteci, T. Balla, and R.F. Irvine. 2012. PI4P and PI(4,5)P<sub>2</sub> are essential but independent lipid determinants of membrane identity. *Science.* 337:727–730. <http://dx.doi.org/10.1126/science.1222483>

- Hardie, R.C. 2003. Regulation of TRP channels via lipid second messengers. *Annu. Rev. Physiol.* 65:735–759. <http://dx.doi.org/10.1146/annurev.physiol.65.092101.142505>
- Hartmann, J., E. Dragicic, H. Adelsberger, H.A. Henning, M. Sumser, J. Abramowitz, R. Blum, A. Dietrich, M. Freichel, V. Flockerzi, et al. 2008. TRPC3 channels are required for synaptic transmission and motor coordination. *Neuron.* 59:392–398. <http://dx.doi.org/10.1016/j.neuron.2008.06.009>
- Hilgemann, D.W. 2007. Local PIP<sub>2</sub> signals: when, where, and how? *Pflugers Arch.* 455:55–67. <http://dx.doi.org/10.1007/s00424-007-0280-9>
- Hill, A.V. 1910. The possible effects of the aggregation of the molecules of haemoglobin on its oxygen dissociation curve. *J. Physiol.* 40:iv–vii.
- Hirose, K., S. Kadowaki, M. Tanabe, H. Takeshima, and M. Iino. 1999. Spatiotemporal dynamics of inositol 1,4,5-trisphosphate that underlies complex Ca<sup>2+</sup> mobilization patterns. *Science.* 284:1527–1530. <http://dx.doi.org/10.1126/science.284.5419.1527>
- Hofmann, T., A.G. Obukhov, M. Schaefer, C. Harteneck, T. Gudermann, and G. Schultz. 1999. Direct activation of human TRPC6 and TRPC3 channels by diacylglycerol. *Nature.* 397:259–263. <http://dx.doi.org/10.1038/16711>
- Hofmann, T., M. Schaefer, G. Schultz, and T. Gudermann. 2002. Subunit composition of mammalian transient receptor potential channels in living cells. *Proc. Natl. Acad. Sci. USA.* 99:7461–7466. <http://dx.doi.org/10.1073/pnas.102596199>
- Horowitz, L.F., W. Hirdes, B.C. Suh, D.W. Hilgemann, K. Mackie, and B. Hille. 2005. Phospholipase C in living cells: Activation, inhibition, Ca<sup>2+</sup> requirement, and regulation of M current. *J. Gen. Physiol.* 126:243–262. <http://dx.doi.org/10.1085/jgp.200509309>
- Imai, Y., K. Itsuki, Y. Okamura, R. Inoue, and M.X. Mori. 2012. A self-limiting regulation of vasoconstrictor-activated TRPC3/C6/C7 channels coupled to PI(4,5)P<sub>2</sub>-diacylglycerol signalling. *J. Physiol.* 590:1101–1119.
- Inoue, R., and H. Kuriyama. 1993. Dual regulation of cation-selective channels by muscarinic and alpha 1-adrenergic receptors in the rabbit portal vein. *J. Physiol.* 465:427–448.
- Inoue, R., L.J. Jensen, J. Shi, H. Morita, M. Nishida, A. Honda, and Y. Ito. 2006. Transient receptor potential channels in cardiovascular function and disease. *Circ. Res.* 99:119–131. <http://dx.doi.org/10.1161/01.RES.0000233356.10630.8a>
- Irvine, R.F., and M.J. Schell. 2001. Back in the water: the return of the inositol phosphates. *Nat. Rev. Mol. Cell Biol.* 2:327–338. <http://dx.doi.org/10.1038/35073015>
- Itsuki, K., Y. Imai, Y. Okamura, K. Abe, R. Inoue, and M.X. Mori. 2012a. Voltage-sensing phosphatase reveals temporal regulation of TRPC3/C6/C7 channels by membrane phosphoinositides. *Channels (Austin).* 6:206–209. <http://dx.doi.org/10.4161/chan.20883>
- Itsuki, K., Y. Imai, Y. Okamura, R. Inoue, and M.X. Mori. 2012b. PIP<sub>2</sub> dynamics underlying muscarinic or vasopressin receptor-activated TRPC3, C6, and C7 currents. *Biophys. J.* 104:454a.
- Jardín, I., P.C. Redondo, G.M. Salido, and J.A. Rosado. 2008. Phosphatidylinositol 4,5-bisphosphate enhances store-operated calcium entry through hTRPC6 channel in human platelets. *Biochim. Biophys. Acta.* 1783:84–97. <http://dx.doi.org/10.1016/j.bbamer.2007.07.007>
- Jensen, J.B., J.S. Lyssand, C. Hague, and B. Hille. 2009. Fluorescence changes reveal kinetic steps of muscarinic receptor-mediated modulation of phosphoinositides and Kv7.2/7.3 K<sup>+</sup> channels. *J. Gen. Physiol.* 133:347–359. <http://dx.doi.org/10.1085/jgp.200810075>
- Kim, Y.J., M.L. Guzman-Hernandez, and T. Balla. 2011. A highly dynamic ER-derived phosphatidylinositol-synthesizing organelle supplies phosphoinositides to cellular membranes. *Dev. Cell.* 21:813–824. <http://dx.doi.org/10.1016/j.devcel.2011.09.005>
- Koenig, S., M. Schernthaner, H. Maechler, C.O. Kappe, T.N. Glasnov, G. Hoefler, M. Braune, E. Wittchow, and K. Groschner. 2013. A TRPC3 blocker, ethyl-1-(4-(2,3,3-trichloroacrylamide)phenyl)-5-(trifluoromethyl)-1H-pyrazole-4-carboxylate (Pyr3), prevents stent-induced arterial remodeling. *J. Pharmacol. Exp. Ther.* 344:33–40. <http://dx.doi.org/10.1124/jpet.112.196832>
- Kosenko, A., S. Kang, I.M. Smith, D.L. Greene, L.K. Langeberg, J.D. Scott, and N. Hoshi. 2012. Coordinated signal integration at the M-type potassium channel upon muscarinic stimulation. *EMBO J.* 31:3147–3156. <http://dx.doi.org/10.1038/emboj.2012.156>
- Kwon, Y., T. Hofmann, and C. Montell. 2007. Integration of phosphoinositide- and calmodulin-mediated regulation of TRPC6. *Mol. Cell.* 25:491–503. <http://dx.doi.org/10.1016/j.molcel.2007.01.021>
- Lemmon, M.A., K.M. Ferguson, and J. Schlessinger. 1996. PH domains: diverse sequences with a common fold recruit signaling molecules to the cell surface. *Cell.* 85:621–624. [http://dx.doi.org/10.1016/S0092-8674\(00\)81022-3](http://dx.doi.org/10.1016/S0092-8674(00)81022-3)
- Lemonnier, L., M. Trebak, and J.W. Putney Jr. 2008. Complex regulation of the TRPC3, 6 and 7 channel subfamily by diacylglycerol and phosphatidylinositol-4,5-bisphosphate. *Cell Calcium.* 43:506–514. <http://dx.doi.org/10.1016/j.ceca.2007.09.001>
- Lo, M.V., and W.L. Pak. 1981. Light-induced pigment granule migration in the retinal cells of *Drosophila melanogaster*. Comparison of wild type with ERG-defective mutants. *J. Gen. Physiol.* 77:155–175. <http://dx.doi.org/10.1085/jgp.77.2.155>
- Loew, L.M. 2007. Where does all the PIP<sub>2</sub> come from? *J. Physiol.* 582:945–951. <http://dx.doi.org/10.1113/jphysiol.2007.132860>
- Logothetis, D.E., T. Jin, D. Lupyán, and A. Rosenhouse-Dantsker. 2007. Phosphoinositide-mediated gating of inwardly rectifying K<sup>+</sup> channels. *Pflugers Arch.* 455:83–95. <http://dx.doi.org/10.1007/s00424-007-0276-5>
- Maruyama, Y., Y. Nakanishi, E.J. Walsh, D.P. Wilson, D.G. Welsh, and W.C. Cole. 2006. Heteromultimeric TRPC6-TRPC7 channels contribute to arginine vasopressin-induced cation current of A7r5 vascular smooth muscle cells. *Circ. Res.* 98:1520–1527. <http://dx.doi.org/10.1161/01.RES.0000226495.34949.28>
- McLaughlin, S., and D. Murray. 2005. Plasma membrane phosphoinositide organization by protein electrostatics. *Nature.* 438:605–611. <http://dx.doi.org/10.1038/nature04398>
- Minke, B. 2010. The history of the *Drosophila* TRP channel: the birth of a new channel superfamily. *J. Neurogenet.* 24:216–233. <http://dx.doi.org/10.3109/01677063.2010.514369>
- Monet, M., N. Francoeur, and G. Boulay. 2012. Involvement of phosphoinositide 3-kinase and PTEN protein in mechanism of activation of TRPC6 protein in vascular smooth muscle cells. *J. Biol. Chem.* 287:17672–17681. <http://dx.doi.org/10.1074/jbc.M112.341354>
- Mori, M.X., Y. Imai, K. Itsuki, and R. Inoue. 2011. Quantitative measurement of Ca<sup>2+</sup>-dependent calmodulin-target binding by Fura-2 and CFP and YFP FRET imaging in living cells. *Biochemistry.* 50:4685–4696. <http://dx.doi.org/10.1021/bi200287x>
- Okada, T., R. Inoue, K. Yamazaki, A. Maeda, T. Kurosaki, T. Yamakuni, I. Tanaka, S. Shimizu, K. Ikenaka, K. Imoto, and Y. Mori. 1999. Molecular and functional characterization of a novel mouse transient receptor potential protein homologue TRP7. Ca<sup>2+</sup>-permeable cation channel that is constitutively activated and enhanced by stimulation of G protein-coupled receptor. *J. Biol. Chem.* 274:27359–27370. <http://dx.doi.org/10.1074/jbc.274.39.27359>
- Okamura, Y., Y. Murata, and H. Iwasaki. 2009. Voltage-sensing phosphatase: actions and potentials. *J. Physiol.* 587:513–520. <http://dx.doi.org/10.1113/jphysiol.2008.163097>
- Panda, S., S.K. Nayak, B. Campo, J.R. Walker, J.B. Hogenesch, and T. Jegla. 2005. Illumination of the melanopsin signaling pathway. *Science.* 307:600–604. <http://dx.doi.org/10.1126/science.11105121>
- Petersson, M.E., M. Yoshida, and E.A. Fransén. 2011. Low-frequency summation of synaptically activated transient receptor potential

- channel-mediated depolarizations. *Eur. J. Neurosci.* 34:578–593. <http://dx.doi.org/10.1111/j.1460-9568.2011.07791.x>
- Prescott, E.D., and D. Julius. 2003. A modular PIP<sub>2</sub> binding site as a determinant of capsaicin receptor sensitivity. *Science*. 300:1284–1288. <http://dx.doi.org/10.1126/science.1083646>
- Ramsey, I.S., M. Delling, and D.E. Clapham. 2006. An introduction to TRP channels. *Annu. Rev. Physiol.* 68:619–647. <http://dx.doi.org/10.1146/annurev.physiol.68.040204.100431>
- Sinnecker, D., and M. Schaefer. 2004. Real-time analysis of phospholipase C activity during different patterns of receptor-induced Ca<sup>2+</sup> responses in HEK293 cells. *Cell Calcium*. 35:29–38. [http://dx.doi.org/10.1016/S0143-4160\(03\)00169-6](http://dx.doi.org/10.1016/S0143-4160(03)00169-6)
- Smedlund, K., J.Y. Tano, and G. Vazquez. 2010. The constitutive function of native TRPC3 channels modulates vascular cell adhesion molecule-1 expression in coronary endothelial cells through nuclear factor kappaB signaling. *Circ. Res.* 106:1479–1488. <http://dx.doi.org/10.1161/CIRCRESAHA.109.213314>
- Soboloff, J., M. Spassova, T. Hewavitharana, L.P. He, P. Luncsford, W. Xu, K. Venkatachalam, D. van Rossum, R.L. Patterson, and D.L. Gill. 2007. TRPC channels: integrators of multiple cellular signals. *Handbook Exp. Pharmacol.* 179:575–591. [http://dx.doi.org/10.1007/978-3-540-34891-7\\_34](http://dx.doi.org/10.1007/978-3-540-34891-7_34)
- Suh, B.C., and B. Hille. 2002. Recovery from muscarinic modulation of M current channels requires phosphatidylinositol 4,5-bisphosphate synthesis. *Neuron*. 35:507–520. [http://dx.doi.org/10.1016/S0896-6273\(02\)00790-0](http://dx.doi.org/10.1016/S0896-6273(02)00790-0)
- Takai, Y., R. Sugawara, H. Ohinata, and A. Takai. 2004. Two types of non-selective cation channel opened by muscarinic stimulation with carbachol in bovine ciliary muscle cells. *J. Physiol.* 559:899–922. <http://dx.doi.org/10.1113/jphysiol.2004.065607>
- Tauseef, M., N. Knezevic, K.R. Chava, M. Smith, S. Sukriti, N. Gianaris, A.G. Obukhov, S.M. Vogel, D.E. Schraufnagel, A. Dietrich, et al. 2012. TLR4 activation of TRPC6-dependent calcium signaling mediates endotoxin-induced lung vascular permeability and inflammation. *J. Exp. Med.* 209:1953–1968. <http://dx.doi.org/10.1084/jem.20111355>
- Tsvilovskyy, V.V., A.V. Zholos, T. Aberle, S.E. Philipp, A. Dietrich, M.X. Zhu, L. Birnbaumer, M. Freichel, and V. Flockerzi. 2009. Deletion of TRPC4 and TRPC6 in mice impairs smooth muscle contraction and intestinal motility in vivo. *Gastroenterology*. 137:1415–1424. <http://dx.doi.org/10.1053/j.gastro.2009.06.046>
- Ufret-Vincenty, C.A., R.M. Klein, L. Hua, J. Angueyra, and S.E. Gordon. 2011. Localization of the PIP<sub>2</sub> sensor of TRPV1 ion channels. *J. Biol. Chem.* 286:9688–9698. <http://dx.doi.org/10.1074/jbc.M110.192526>
- van den Bogaart, G., K. Meyenberg, H.J. Risselada, H. Amin, K.I. Willig, B.E. Hubrich, M. Dier, S.W. Hell, H. Grubmüller, U. Diederichsen, and R. Jahn. 2011. Membrane protein sequestering by ionic protein-lipid interactions. *Nature*. 479:552–555. <http://dx.doi.org/10.1038/nature10545>
- van der Wal, J., R. Habets, P. Várnai, T. Balla, and K. Jalink. 2001. Monitoring agonist-induced phospholipase C activation in live cells by fluorescence resonance energy transfer. *J. Biol. Chem.* 276:15337–15344. <http://dx.doi.org/10.1074/jbc.M007194200>
- van Rossum, D.B., R.L. Patterson, S. Sharma, R.K. Barrow, M. Kornberg, D.L. Gill, and S.H. Snyder. 2005. Phospholipase Cgamma1 controls surface expression of TRPC3 through an intermolecular PH domain. *Nature*. 434:99–104. <http://dx.doi.org/10.1038/nature03340>
- Venkatachalam, K., and C. Montell. 2007. TRP channels. *Annu. Rev. Biochem.* 76:387–417. <http://dx.doi.org/10.1146/annurev.biochem.75.103004.142819>
- Violin, J.D., J. Zhang, R.Y. Tsien, and A.C. Newton. 2003. A genetically encoded fluorescent reporter reveals oscillatory phosphorylation by protein kinase C. *J. Cell Biol.* 161:899–909. <http://dx.doi.org/10.1083/jcb.200302125>
- Weissmann, N., A. Sydykov, H. Kalwa, U. Storch, B. Fuchs, M. Mederos y Schnitzler, R.P. Brandes, F. Grimminger, M. Meissner, M. Freichel, et al. 2012. Activation of TRPC6 channels is essential for lung ischaemia-reperfusion induced oedema in mice. *Nat. Commun.* 3:649. <http://dx.doi.org/10.1038/ncomms1660>
- Winks, J.S., S. Hughes, A.K. Filippov, L. Tatulian, F.C. Abogadie, D.A. Brown, and S.J. Marsh. 2005. Relationship between membrane phosphatidylinositol-4,5-bisphosphate and receptor-mediated inhibition of native neuronal M channels. *J. Neurosci.* 25:3400–3413. <http://dx.doi.org/10.1523/JNEUROSCI.3231-04.2005>
- Xie, J., B. Sun, J. Du, W. Yang, H.C. Chen, J.D. Overton, L.W. Runnels, and L. Yue. 2011. Phosphatidylinositol 4,5-bisphosphate (PIP<sub>2</sub>) controls magnesium gatekeeper TRPM6 activity. *Sci. Rep.* 1:146. <http://dx.doi.org/10.1038/srep00146>
- Yudin, Y., V. Lukacs, C. Cao, and T. Rohacs. 2011. Decrease in phosphatidylinositol 4,5-bisphosphate levels mediates desensitization of the cold sensor TRPM8 channels. *J. Physiol.* 589:6007–6027. <http://dx.doi.org/10.1113/jphysiol.2011.220228>
- Zacharias, D.A., J.D. Violin, A.C. Newton, and R.Y. Tsien. 2002. Partitioning of lipid-modified monomeric GFPs into membrane microdomains of live cells. *Science*. 296:913–916. <http://dx.doi.org/10.1126/science.1068539>